Investigation of the cytotoxic potential of methyl imidazole-derived thiosemicarbazones and their copper(II) complexes with dichloroacetate as a co-ligand†

Oleg Palamarciuc,[a] Miljan N. M. Milunović, [ID] *[bc] Angela Sîrbu,[a] Elena Stratulat,[a] Aurel Pui,[d] Nevenka Gligorijevic,[e] Sinisa Radulovic,[e] Jozef Kožíšek,[c] Denisa Darvasiová,[c] Peter Rapta,[c] Eva A. Enyedy, [ID] [f] Ghenadie Novitchi,[g] Sergiu Shova[h] and Vladimir B. Arion [ID] *[b]

A series of six imidazole-derived thiosemicarbazones (**HL¹–HL⁶**) and their copper(II) complexes (**1–6**) were synthesised and characterised by analytical, spectroscopic, electrochemical and single crystal X-ray diffraction techniques. In addition, solution studies and the results of antiproliferative activity in human cancer cell lines with some insights into the mechanism of cancer cell death are also reported. In particular, the substitution of one hydrogen at the terminal N-atom of the thiosemicarbazide moiety by a phenyl group resulted in slightly enhanced antiproliferative activity. **HL³** and **HL⁶** showed lower IC₅₀ values compared to **HL¹** and **HL⁴** in MDA-MB-453 and LS174 cancer cell lines. The copper(II) complexes **3** and **6** exhibit a 2.4- and 4.7-fold increase of activity compared to parent proligands in MDA-MB-453 cancer cell line, respectively. The complex formation of the proligands with copper(II) increased their antiproliferative activity in all investigated cell lines. The cell cycle perturbations, apoptotic potential and the analysis of morphological changes in the A549 cell line induced by **3** and **6** revealed cytostatic rather than cytotoxic effects.

1 Introduction

The thiosemicarbazide moiety is a key pharmacophore of many agents with anticancer activity. The most studied thiosemi-carbazide derivative so far is 3-aminopyridine-2-carboxaldehyde thiosemicarbazone (Triapine). Despite its remarkable cytotoxic activity *in vitro* and *in vivo*, clinical investigations showed mixed results.[1–5] Recently, two thiosemicarbazones (TSCs) of a new generation, namely di-2-pyridylketone 4-cyclohexyl-4-methyl-3-thiosemicarbazone (DpC) and (*E*)-*N'*-(6,7-dihydroquinolin)-8((5*H*)-ylidene)-4-(pyridine-2-yl)piperazine-1-carbothio-hydrazide (COTI-2), have entered clinical studies, rekindling the interest for this class of compounds.[6,7] Regardless of their broad biological/pharmacological potency and multitarget features, TSCs act as excellent metal chelators, often exhibiting enhanced biological activity upon coordination to metal ions.[8]

Copper, as an essential micronutrient in the human body, plays an important role in metabolic processes (oxygen transport, cell signaling and enzyme activity).[9] Besides its biological importance, copper increases the cytotoxic effect of many thiosemicarbazones upon coordination.[10–13] Copper(II)-thiosemi-carbazonates exhibit remarkable antiproliferative activity in various cancer cell lines,[10,11,13] inhibit the topoisomerase II enzyme[14,15] and/or induce apoptosis.[13]

The mechanism of action of copper(II)-thiosemicarbazonates is often closely related to apoptosis caused by (i) the inhibition of the important enzymes often overexpressed in cancer cells, (ii) formation of free radicals (reactive oxygen species (ROS)) due to the redox activity of copper, which damage important

[a] *Moldova State University, Department of Chemistry, A. Mateevici Street 60, MD-2009 Chisinau, Republic of Moldova*

[b] *University of Vienna, Faculty of Chemistry, Institute of Inorganic Chemistry, Währinger Strasse 42, A-1090, Austria. E-mail: miljan.milunovic@univie.ac.at, vladimir.arion@univie.ac.at*

[c] *Slovak University of Technology, Faculty of Chemical and Food Technology, Institute of Physical Chemistry and Chemical Physics, Radlinského 9, SK-812 37 Bratislava, Slovakia*

[d] *Faculty of Chemistry, University "Alexandru Ioan Cuza", 11, Carol I Boulevard, 700506 Iasi, Romania*

[e] *Institute for Oncology and Radiology of Serbia, Pasterova 14, 11000 Belgrade, Serbia*

[f] *Department of Inorganic and Analytical Chemistry, University of Szeged, Dom ter 7, H-6720 Szeged, Hungary*

[g] *Laboratoire National des Champs Magnetiques Intenses-CNRS, 25 Avenue des Martyrs, 38042 Grenoble Cedex 9, France*

[h] *'Petru Poni' Institute of Macromolecular Chemistry, Aleea Gr. Ghica Voda 41A, 700487 Iasi, Romania*

† Electronic supplementary information (ESI) available. CCDC 1577585 (**1**), 1845470 (**2**), 1845471 (**3**), 1845472 (**4**), 1845473 (**5**), 1845474 (**6**). For ESI and crystallographic data in CIF or other electronic format see DOI: 10.1039/c8nj04041a

biomolecules (enzymes, DNA) and (iii) DNA intercalation.[13,16–18] Neutral and cationic copper(II) bis(thiosemicarbazone) complexes with methyl and phenyl substituents caused DNA cleavage and inhibition of topoisomerase II and inhibited tumour growth when administered *in vivo*.[19]

The imidazole moiety is imbedded into the structures of important biological compounds (*e.g.*, histidine) and it is a central pharmacophore in many antiviral, antifungal and anti-cancer agents.[20] Recent studies on imidazole-derived thiosemi-carbazones showed an antiproliferative effect on bacteria, which is enhanced upon coordination to copper(II). Polyphar-macological effects, *e.g.*, cytotoxic and antimicrobial activity,[21] were also noticed for other compounds.[22]

Dichloroacetic acid (DCA) interrupts mitochondrial function by inhibiting pyruvate dehydrogenase and does not have a toxic effect on normal cells.[23] At the same time DCA exhibits antiproliferative activity in T-cell lymphoma,[24] small-cell lung,[25] prostate,[26] colorectal[27] and breast carcinoma cells,[28] when applied separately or in combination with other approved chemotherapeutics such as platinum-based drugs,[29] 5-fluoro-uracil,[30] bortezomib,[31] sorafenib,[32] and bevacizumab.[33] Quite recently, DCA entered phase I clinical trials as a potential agent against brain tumours upon oral administration.[34] A copper(II) thiosemicarbazonate co-crystallised with DCA was reported as an effective antiproliferative agent against breast cancer cells.[35]

A fusion of dichloroacetate with copper(II) complexes based on imidazole-carboxaldehyde thiosemicarbazone in one com-pound might be of interest for the development of dual-action anticancer drugs.

Herein we report on the synthesis and characterisation of methyl imidazole-derived thiosemicabazones **HL¹** and **HL⁴** and their *N*-methyl and *N*-phenyl substituted analogues **HL²**, **HL³**, **HL⁵** and **HL⁶** as shown in Chart 1, as well as of their copper(II) complexes **1–6** with dichloroacetate as a co-ligand, shown in Chart 2.

In addition, complex formation with copper(II) in solution, the electrochemical behaviour of the copper(II) complexes and the antiproliferative activity of proligands **HL¹⁻⁶** and their copper(II) complexes **1–6** in human lung adenocarcinoma cells (A549), colon cancer cells (LS174), breast carcinoma cells (MDA-MB-453) and human bronchial epithelial cells (BEAS-2B) were investigated. Finally, the apoptotic potential and the mechanism of cell demise of the most active complexes **3** and **6** in lung adenocarcinoma cells (A549) are reported.

2 Results and discussion

2.1 Synthesis and characterisation of proligands HL¹⁻⁶ and the copper(II) complexes 1–6

All proligands were obtained in high yields by a condensation reaction of 2-methyl-1*H*-imidazole-4-carboxaldehyde or 5-methyl-1*H*-imidazole-5-carboxaldehyde with thiosemicarbazide or its N⁴-substituted derivative in absolute ethanol under reflux. The products were characterised by elemental analyses, which were in agreement with expected compositions, ESI mass spectro-metry, one- and two-dimensional NMR spectroscopy, UV-vis and IR spectroscopy. Positive ion ESI mass spectra showed peaks with *m/z* values attributed to [HL + H]⁺ and [HL + Na]⁺ ions,
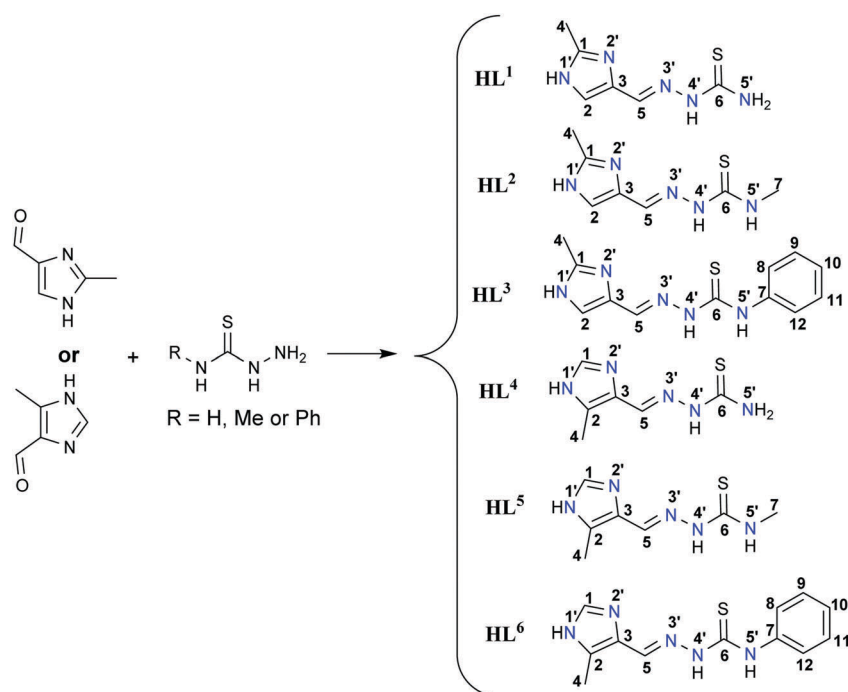

Chart 1 Synthesis and line drawings of proligands **HL¹⁻⁶**. Reaction conditions: EtOH, reflux, 2 h. The atom labelling is used for NMR resonance assignment.
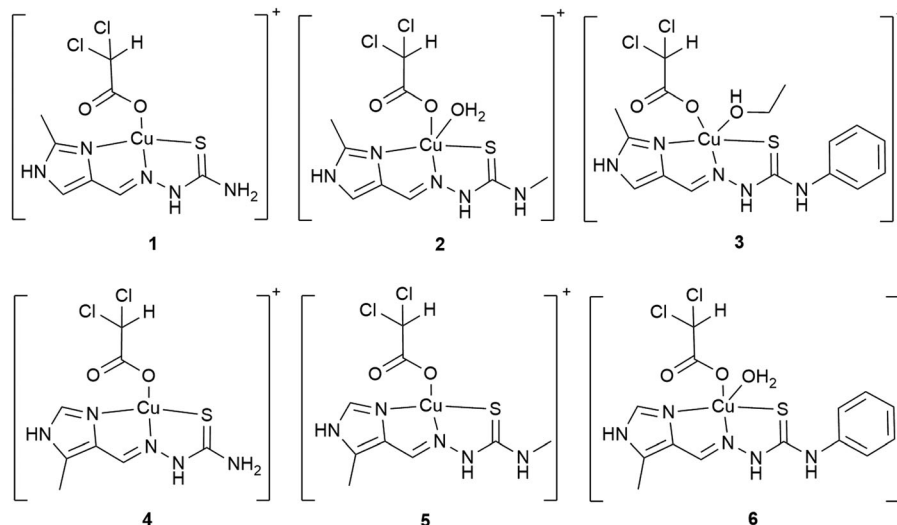
Chart 2 Line drawings of copper(ii) complexes **1–6**. Dichloroacetate as a counteranion and co-crystallised ethanol molecules were omitted for the sake of clarity.

namely 184 and 206 for HL^1 and HL^4, 198 and 220 for HL^2 and HL^5, and 260 and 282 for HL^3 and HL^6, while in negative ion mode spectra peaks with m/z 182 attributed to $[L^1]^-$ and $[L^4]^-$, 196 to $[L^2]^-$ and $[L^5]^-$, and 258 to $[L^3]^-$ and $[L^6]^-$ were observed.

The existence of E and Z isomers in solution was confirmed by two sets of signals in 1D (^{1}H and ^{13}C) and 2D (COSY, HSQC, HMBC) NMR spectra in $(CD_3)_2SO$ (see ESI†). Geometric isomerism is typical for thiosemicarbazones and our data are in good agreement with those reported for other imidazole-thiosemi-carbazones.[36–40] The population ratio is 1:1 for all proligands in $(CD_3)_2SO$ reflecting the statistical distribution of E and Z isomers, except HL^2, for which the Z isomer is favoured ($Z:E$ = 1:0.26). It should be also noted that isomerisation is accompanied by proton exchange processes (involving DHO present in $(CD_3)_2SO$). These exchange processes strongly affect the relaxation times of particular nuclei and, as a consequence, some ^{13}C signals were not detected. More affected are the Z isomers implying their higher lability when compared to the E isomers. Additionally, significant differences in chemical shifts (up to ∼1 ppm) for the imine protons were observed (see ESI†). The higher lability of Z over E isomers, along with the large difference in the chemical shifts for some protons, indicates not only Z/E isomerism in solution, but also the acid–base tautomerism of imidazole rings as depicted in Chart 3 for HL^1.

The copper(ii) complexes **1–6** were obtained by reaction of an appropriate thiosemicarbazone with $Cu_2(OH)_2CO_3$ and dichloroacetic acid in a 2:1:2 molar ratio in aqueous ethanol under reflux. Green raw products, separated from solution upon standing at room temperature within 3–4 days, were re-crystallised in ethanol. The compounds were characterised by UV-vis, IR spectroscopy and ESI mass spectrometry. Electronic absorption spectra showed characteristic intraligand bands with maxima between 300 and 380 nm and metal-to-ligand charge transfer and d–d transition (low extinction coefficients) bands in the range 550–750 nm (see ESI,† Fig. S8). ESI-MS measurements
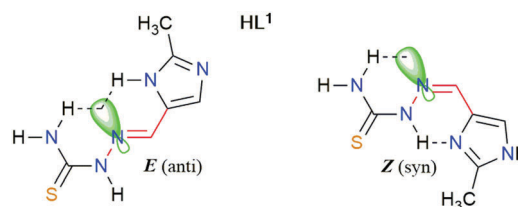

Chart 3 Geometric E/Z isomerism, tautomerism of the imidazole ring and H-bonding interactions in HL^1.

in positive ion mode showed peaks attributed to ions $[Cu^{II}(L^{1–6})]^+$ and $[Cu^{II}_2(L^{1–6})_2(CHCl_2CO_2)]^+$, while in negative ion mode peaks with m/z values (see Experimental section) which could be assigned to ions $[Cu^{II}(L^{1–6}–H)(CHCl_2CO_2)]^-$ and $[Cu^{II}_2(L^{1–6}–H)_2(CHCl_2CO_2)]^-$. ESI mass spectra of a methanolic solution of **6** with an excess of DMSO measured immediately after sample preparation showed a major peak at m/z 771 assigned to $[Cu^{II}_2(L^6)_2(CHCl_2CO_2)]^+$ and a minor peak at m/z 399 which can be attributed to $[Cu(L^6)DMSO]^+$. The general picture did not change after 24 h, indicating that replacement of the dichloracetato co-ligand ($CHCl_2CO_2^-$) by DMSO is not time-dependent and a favoured transformation (see ESI†). The compounds crystallised in ethanol proved to be suitable for single crystal X-ray crystallography studies.

2.2 X-ray crystallography (description of the crystal structure of 1–6)

The results of X-ray diffraction studies of **1–6** are shown in Fig. 1 and 2, while bond distances and bond angles are quoted in Tables S1–S7 (ESI†). All six compounds have an ionic crystal structure, which is built up from the complex cations $[Cu(HL^{1–6})(CHCl_2CO_2)]^+$ and dichloroacetate counteranion in 1:1 stoichiometry (Fig. 1 and 2). There are no co-crystallised solvent molecules in **1**, **3** and **4**, while **2**, **5** and **6** crystallise with one water or ethanol molecule per copper(ii) complex.
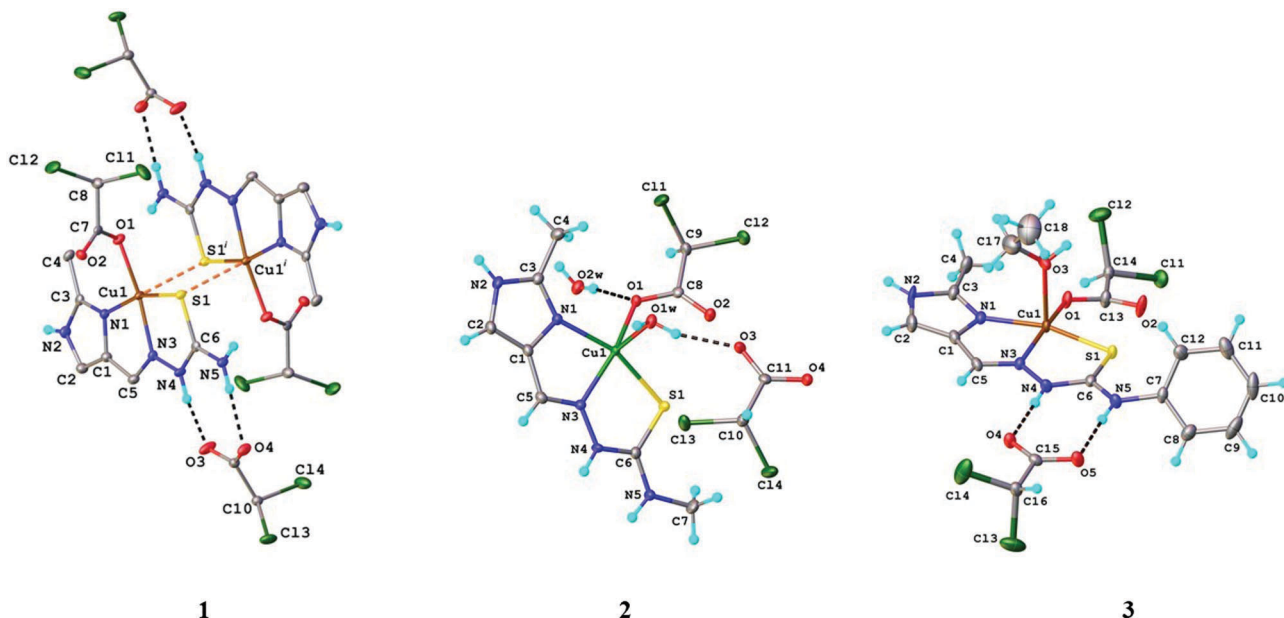
Fig. 1 Extended asymmetric unit and coordination environment around the Cu(II) ion in **1**, **2** and **3** with atom labelling and thermal ellipsoids at 50% probability level. H-Bond parameters for **1**: N4–H···O3 [N4–H 0.88 Å, H···O3 1.76 Å, N4···O3 2.615(2) Å, N4–H···O3 165.1°]; N5–H···O4 [N5–H 0.88 Å, H···O4 2.02 Å, N5···O4 2.895(2) Å, N5–H···O4 174.7°]. Symmetry code: (i) 1 − x, −y, −z. H-Bond parameters for **2**: O1w–H1w···O3 [O1w–H 0.82 Å, H1w···O3 1.99 Å, O1w···O3 2.790(2) Å, O1w–H1w···O3 165.2°]; O2w–H2w···O1 [O2w–H2w 0.83 Å, H2w···O1 2.00 Å, O2w···O1 2.825(19) Å, O2w–H2w···O1 170.9°]. H-Bond parameters for **3**: N4–H···O4 [N4–H 0.88 Å, H···O4 1.81 Å, N4···O4 2.688(3) Å, N4–H···O4 175.1°]; N5–H···O5 [N5–H 0.88 Å, H···O5 1.88 Å, N5···O5 2.763(3) Å, N5–H···O5 175.9°].
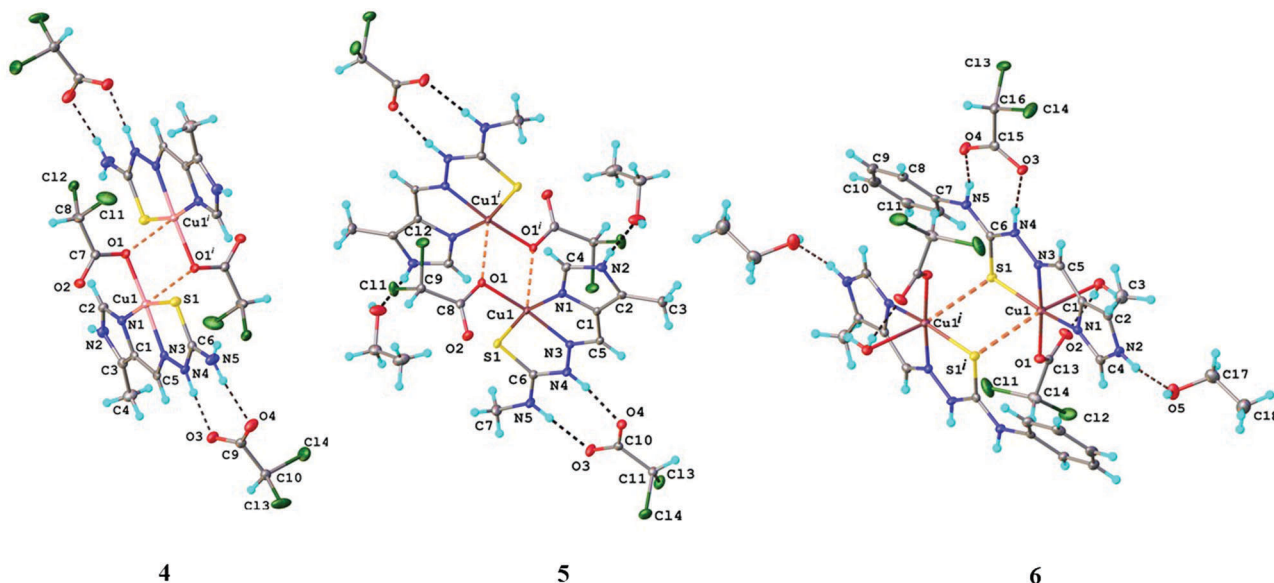

Fig. 2 Extended asymmetric unit and coordination environment of copper(II) in **4**–**6** with atom labelling and thermal ellipsoids at 50% probability level. H-Bond parameters for **4**: N4–H···O3 [N4–H 0.88 Å, H···O3 1.76 Å, N4···O3 2.638(2) Å, N4–H···O3 173.2°]; N5–H···O4 [N5–H 0.88 Å, H···O4 1.97 Å, N5···O4 2.800(2) Å, N5–H···O4 168.6°]. Symmetry code: (i) −x, 1 − y, 1 − z. H-Bond parameters for **5**: N4–H···O4 [N4–H 0.88 Å, H···O4 1.84 Å, N4···O4 2.701(2) Å, N4–H···O4 164.9°]; N5–H···O3 [N5–H 0.88 Å, H···O3 1.88 Å, N5···O3 2.761(2) Å, N5–H···O3 177.1°]. Symmetry code: (i) 1 − x, 1 − y, 1 − z. H-Bond parameters for **6**: N4–H···O3 [N4–H 0.88 Å, H···O3 1.82 Å, N4···O3 2.693(2) Å, N4–H···O3 171.2°]; N5–H···O4 [N5–H 0.88 Å, H···O4 1.92 Å, N5···O4 2.785(2) Å, N5–H···O4 165.5°]; N2–H···O5 [N2–H 0.88 Å, H···O5 1.88 Å, N2···O5 2.746(2) Å, N2–H···O5 166.5°]. Symmetry code: (i) 1 − x, −y, 2 − z.

The thiosemicarbazones $HL^{1–6}$ in the structures **1**–**6** act as neutral tridentate ligands and bind to copper(II) via NNS donor atoms. In complexes **1**, **4** and **5** the copper(II) ion adopts a slightly distorted square-planar coordination geometry, which is completed by monodentate binding of the $CHCl_2CO_2^−$ anion. The coordination environment of the copper(II) atom in **2**, **3**

and **6** is five-coordinate and can be described as distorted square-pyramidal. In addition to the tridentate ligands **HL²**, **HL³** and **HL⁶** in **2**, **3** and **6**, the central copper(II) atom is bound by the monodentate $CHCl_2CO_2^-$ anion in the base of the pyramid and by a C_2H_5OH or H_2O molecule in the apical position (Fig. 1 and 2).

The displacement of the Cu(II) ion from the basal plane towards the apical position is equal to 0.269, 0.153 and 0.129 Å, for **2**, **3** and **6**, respectively. Selected bond distances, showing the geometry of the coordination environment, are given in Table S1 (ESI†). It is of note that the copper(II) in all complexes (except **2** and **3**) is additionally coordinated by a donor atom from an adjacent unit with formation of a centrosymmetric dinuclear cationic species (Fig. 1, 2 and Fig. S1–S6, ESI†) with a $Cu \cdots Cu'$ separation of 3.619(2) Å, 3.445(2) (molecule A) and 3.5443(2) Å (molecule B), 3.5320(2) Å and 3.9659(1) Å for **1**, **4**, **5** and **6**, respectively. In two cases (**1** and **6**), additional coordination or weak interaction is provided by the sulfur atom of the thiosemicarbazide moiety with a $Cu1 \cdots S1'$ distance of 2.8274(2) Å and 3.2035(9) Å for **1** and **6**, respectively, and by the oxygen atom from the coordinated $CHCl_2CO_2^-$ anion in **4** ($Cu1 \cdots O'$ 2.5134(2) Å (for molecule A) and 2.5240(2) Å (for molecule B)) and in **5** ($Cu1 \cdots O'$ 2.5244(1) Å). Of note is the formation of dimeric associates in **1** through the thioamide S atoms of neutral **HL¹**.[41] The building of such dimers is more common for copper(II) complexes with anionic (iminothiolate) thiosemicarbazonato ligands.[42,43] The packing of the studied complexes is determined by intermolecular hydrogen bonding interactions due to the presence of various proton-donors, *e.g.*, NH groups of imidazole and thiosemicarbazide moieties, and proton-acceptor groups, *e.g.* OH, provided by coordinated solvent molecules. In particular, the formation of 2D supramolecular architectures is of note in the majority of complexes except crystal **2**, which shows the formation of a rather elaborate 3D supramolecular network, and **5**, the crystal structure of which is characterized as the packing of isolated supramolecular ribbons. Views of parts of the crystal structure for **1–6** are shown in Fig. S9–S14 (ESI†), respectively.

The thermodynamic stability of the complexes characterised in the solid state by X-ray crystallography was further investigated in aqueous solution.

2.3 Solution equilibrium studies (protonation of proligands HL¹ and HL⁴ and copper(II) complex formation)

In order to characterise the protonation/proton dissociation of proligands **HL¹** and **HL⁴**, as well as copper(II) complex formation with **HL¹** and **HL⁴** as ligands, UV-vis spectrophotometric titrations were performed by using aqueous solutions. The measured spectra revealed characteristic changes in the monitored wavelength range upon increasing the pH, especially in the basic pH range (see Fig. 3 for **HL¹**). The pH-dependence of the absorbance values showed two well-separated deprotonation steps at pH 4.2–7.0 and 10.0–12.2 for both proligands studied. Therefore, two protonation constants (pK_a values) could be determined on the basis of the deconvolution of the measured spectra (Table 1).
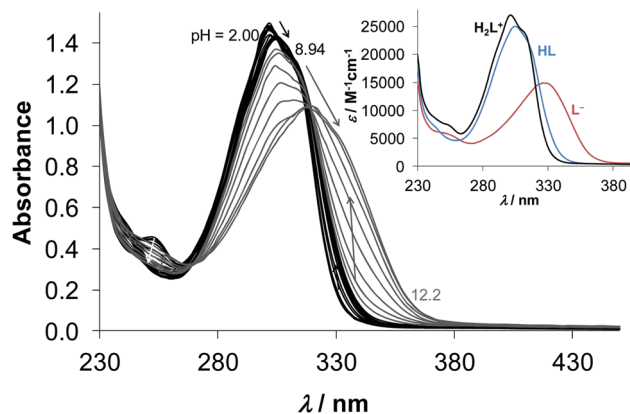

Fig. 3 UV-vis spectra of **HL¹** recorded in the pH range 2–12.2. Inset shows the calculated molar absorbance spectra of the proligand species in the different protonation states (c_{ligand} = 49 μM; I = 0.10 M (KCl); T = 298 K).

Table 1 Protonation ($\log \beta H_iL$) and proton dissociation constants (pK_a) of the ligands **HL¹** and **HL⁴**, λ_{max} and molar absorptivity (ε) values of the ligand species and conditional ($\log \beta_{4.07}'$ [CuL]⁺) and overall stability constants ($\log \beta$ [CuL]⁺) of the copper(II) complexes (I = 0.10 M (KCl); T = 298 K)

Proligand	HL¹	HL⁴
$\log \beta$ HL	11.6 ± 0.1	11.6 ± 0.1
$\log \beta$ H₂L⁺	17.19 ± 0.04	16.89 ± 0.04
pK_1	5.64	5.34
pK_2	11.6	11.6
λ_{max}, nm (ε, M⁻¹ cm⁻¹) H₂L⁺	302 (2.70 × 10⁴)	302 (2.98 × 10⁴)
λ_{max}, nm (ε, M⁻¹ cm⁻¹) HL	304 (2.50 × 10⁴)	308 (2.95 × 10⁴)
λ_{max}, nm (ε, M⁻¹ cm⁻¹) L⁻	328 (1.49 × 10⁴)	332 (1.85 × 10⁴)
$\log \beta'$ [CuL]⁺ at pH 4.07[a]	8.6 ± 0.1	8.88 ± 0.06
$\log \beta$ [CuL]⁺ [b]	17.6	17.65

[a] Determined by UV-vis spectroscopy *via* competition studies with EDTA. Protonation constants of EDTA and stability constants of its copper(II) complex are taken from the literature.[45] $\log \beta$ values: 10.26 (HL), 16.42 (H₂L), 19.09 (H₃L), 21.08 (H₄L), 18.7 (CuL). $\log \beta'$ of (CuL): 10.40 at pH 4.07. [b] Calculation of the overall stability constants of the [CuL]⁺ complexes (β) from the conditional stability constants (β' at pH 4.07): $\beta = \beta' \times \alpha_H$, where $\alpha_H = 1 + [H^+] \times \beta HL + [H^+]^2 \times \beta H_2L^+$; $[H^+] = 10^{-4.07}$.

The protonated proligands possess two proton dissociable groups, namely the imidazole $N^{2'}H^+$ and the hydrazine $N^{4'}–H$ of the thiosemicarbazide moiety. pK_1 and pK_2 can be attributed to the deprotonation of the imidazole and the hydrazine nitrogens, respectively. Notably, the negative charge is mainly localised on the S atom in the deprotonted (**L¹**)⁻ or (**L⁴**)⁻ forms *via* the thione/thiol tautomeric equilibrium as shown in Chart 4. The values of pK_2 are rather uncertain as the second deprotonation step takes place partly in the pH range where the measurement of pH became less accurate (pH > 11.5) due to the alkaline error of the glass electrode. The calculated individual spectra of the proligand species (shown for **HL¹** in Fig. 3) present strong similarity between the absorption of species H₂L⁺ and HL, while spectra of HL and L⁻ are significantly different. The pK_a values of proligands **HL¹** and **HL⁴** are similar to each other, although pK_1 is somewhat lower for **HL⁴**. pK_a values of the best-known α-N-pyridyl thiosemicarbazone, triapine, were reported in our previous work only in
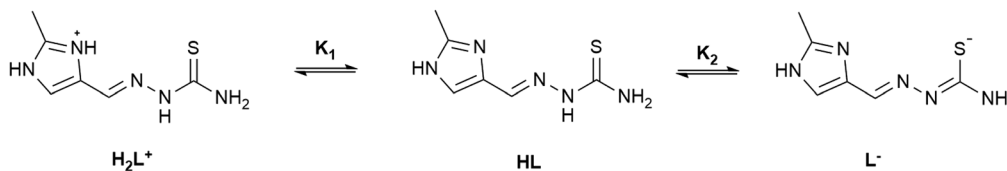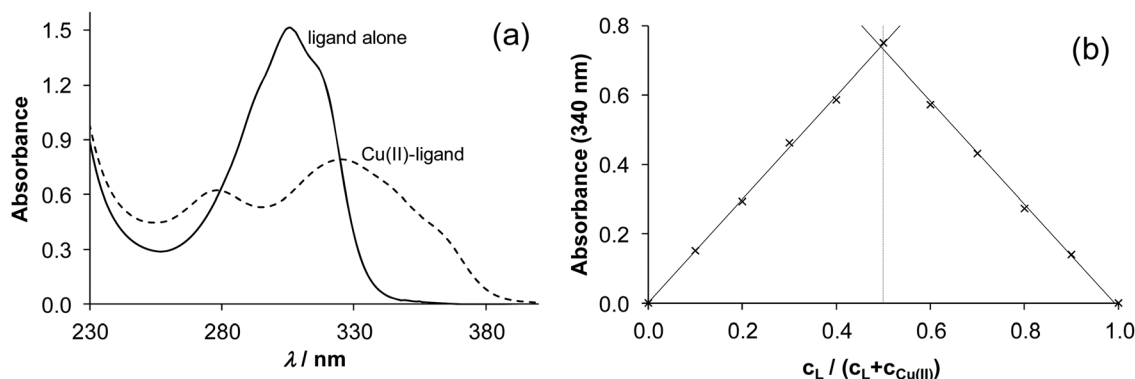
Chart 4 Deprotonation steps of $(H_2L^1)^+$.

Fig. 4 Changes of UV-vis spectra of HL^4 (solid line) (a) upon addition of 1 equiv. of Cu(II) (dashed line) at a constant pH (pH = 3.75; c_{ligand} = 38.7 μM); (b) dependence of absorbance values at 340 nm $vs.$ ratio of c_{ligand} to $c_{ligand} + c_{Cu(II)}$ at a constant pH and constant $c_{ligand} + c_{Cu(II)}$ (pH = 4.07; $c_{ligand} + c_{Cu(II)}$ = 100 μM).

the presence of 30% (w/w) DMSO.[44] However, data obtained in different media cannot be compared directly. Nevertheless, the undoubtedly higher pK_a of the hydrazine nitrogen in the studied herein proligands HL^1 and HL^4 (Table 1) compared to that of triapine (10.78) is obvious. In addition, the pK_a of the imidazole nitrogen is also higher than that of the pyridinium nitrogen in triapine (3.92). Based on the determined pK_a values it can be concluded that both proligands, and most probably the other derivatives studied herein as well, are present in their neutral HL form at physiological pH.

The complex formation with copper(II) is well-indicated by the development of the characteristic S → Cu charge transfer band with a maximum at 321 and 327 nm in the case of HL^1 and HL^4 (Fig. 4a), respectively. The absorbance values at these wavelengths show pH-dependence most probably due to the protonation of the complex at the hydrazine nitrogen in the acidic pH range and due to the formation of mixed hydroxido complexes in the basic pH range, as it was found for copper(II) complexes of numerous α-N-heterocyclic thiosemicarbazones, $e.g.$, triapine or 2-formylpyridine TSC, or further deprotonation of the thiosemicarbazone.[38,44] The latter is supposed to take place only under the conditions of ESI MS measurements (see Experimental). The titration data indicate that the optimal window for the complex formation between HL^1 or HL^4 and the metal ion resulting in $[CuL]^+$ type species is between pH 3.3 and 4.5. First, methods of continuous variation (Fig. 4b) and molar ratios were applied to establish the stoichiometry and stability of the complex formed. The data suggest building of 1:1 complexes (as there was no indication for the formation of bis-ligand to metal complexes at ligand excess), which is practically quantitative under the applied conditions (pH 4.07).

This latter finding hindered the direct determination of the apparent (conditional) formation constants (β') of the copper(II) complexes.

In order to determine the β' values for the $[CuL]^+$ complexes, competition reactions with EDTA were performed at pH 4.07 using spectrophotometry (Fig. 5). It should be noted that EDTA, its copper(II) complex and the unbound TSC ligand have negligible contribution to the measured absorbance values at the chosen wavelengths, namely 337 nm for HL^1 and 340 nm for HL^4.

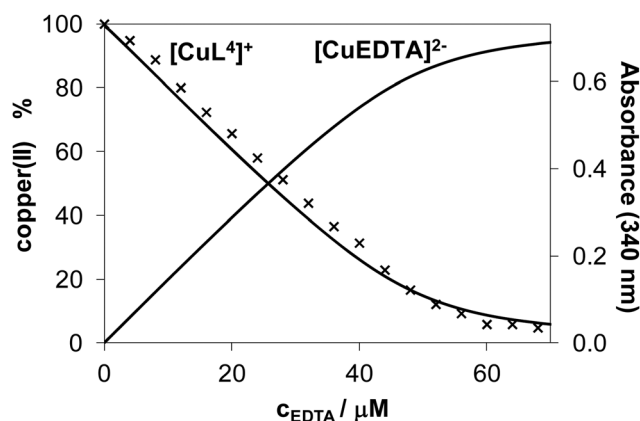The determined conditional formation constants are quoted in Table 1. These constants are fairly similar to each other.

Fig. 5 Concentration distribution for the Cu(II)−HL^4−EDTA system at pH 4.07 at various EDTA concentrations together with the recorded absorbance values at 340 nm (c_{ligand} = 50 μM; $c_{Cu(II)}$ = 50 μM; c_{EDTA} = 0−70 μM; I = 0.10 M (KCl); T = 298 K).

The constant for $[Cu(L^4)]^+$ is slightly higher than that of $[Cu(L^1)]^+$. By using the protonation constants of the proligands the overall stability constants (β) of the complexes $[CuL]^+$ could be also calculated from the conditional stability constants determined (Table 1). These constants reflect the formation of high stability copper(II) complexes with α-N-imidazole-carboxaldehyde thiosemicarbazones used in this study. UV-vis spectra for the copper(II)–HL^1 (or HL^4) systems were recorded in a wide concentration range (10 to 100 μM) and the observed linear dependence (see Fig. S15, ESI,† for HL^1) indicates the high solution stability of the metal complexes at the studied pH.

2.4 Electrochemistry

Cyclic voltammograms of **1–6** measured in DMSO/nBu$_4$NPF$_6$ using a Pt working electrode are very similar to each other and show one reduction peak and a strongly shifted reoxidation peak at a scan rate of 100 mV s^{-1} as shown for **4–6** in Fig. 6 and **1–3** in Fig. S16 (ESI†). The first reduction step is supposed to be metal-centred and can be attributed to the Cu^{II} → Cu^{I} process. The cathodic peak potentials E_{pc} of **4–6** are −0.83 V, −0.83 V, and −0.86 V vs. Fc$^+$/Fc (−0.19 V, −0.19 V, and −0.22 V vs. NHE), respectively. These low redox potentials clearly occur within the biologically accessible window (−0.4 to +0.8 V vs. NHE) using the known $E_{1/2}$ of ferrocene (+0.64 V) versus the standard hydrogen electrode (SHE).[46]

A large peak-to-peak separation (around 600 mV) indicates a slow electron transfer. This was confirmed by experiments at different scan rates (Fig. 7), where by decreasing the scan rate the peak-to-peak separation decreases.

As can be seen in Fig. 7c the peak current for the electrochemical reduction of **6** shows a linear dependence vs. the square root of the scan rate, indicating a diffusion controlled reduction process.[47,48] However, the dependence of the anodic peak current vs. the square root of the scan rate is not linear
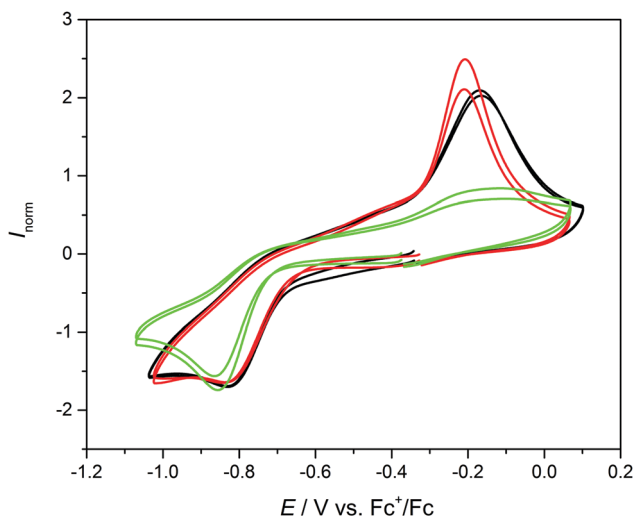
(Fig. 7d). The successful simulation of the corresponding cyclic voltammograms confirmed the slow electrode kinetics (k_s = 0.9 × 10^{-5} cm s^{-1}) and adsorption of the less soluble reduced Cu^{I} species (Γ_{max} = 3.7 × 10^{-9}) on the electrode surface.[49–51] An example of simulated CV is shown for **6** in Fig. S17 (ESI†). In addition, the simulation enabled the determination of the formal redox potential for **6** with $E^{\circ\prime}$ = −0.48 V vs. Fc$^+$/Fc (see Table S8, ESI†).

These studies indicate that potentially compounds **1–6** can be reduced by biological reductants and generate ROS under the conditions of MTT assays, which often induce apoptosis of cancer cells by damaging DNA[52] or other biomolecules[53] as reported for related thiosemicarbazones. The reduction of Cu(II) to Cu(I) for complexes with redox potentials in a biologically relevant window is feasible. The reoxidation of Cu(I) with molecular oxygen could lead to formation of superoxide species (O$_2^{\bullet-}$). EPR spin-trapping experiments and plasmid-DNA cleavage provide evidence of ROS formation.[54,55] H$_2$O$_2$ can be generated by dismutation. Cu$^+$ is able to convert H$_2$O$_2$ to OH$^{\bullet}$ radicals, while O$_2^{\bullet-}$ can also reduce Cu^{2+} to Cu$^+$.[56]

On the other hand, there are copper(II) thiosemicarbazone complexes with redox activity in a biologically relevant window which neither induce generation of ROS nor show apoptotic potential.[8a,57]

2.5 Antiproliferative activity, and cytostatic and cytotoxic potency

Results of MTT assay. The cell growth inhibition activity of the proligands HL^{1-6} and their copper(II) complexes **1–6** against four human cancer cell lines, namely lung adenocarcinoma (A549), colon cancer (LS174), breast carcinoma (MDA-MB-453) and normal bronchial epithelial cells (BEAS-2B), was determined by MTT assay. The proligands with phenyl substituents at the terminal N atom of the thiosemicarbazide moiety, HL^3 and HL^6, showed IC$_{50}$ values <100 μM in LS174, and MDA-MB-453 cell lines (Table 2) with slightly elevated cytotoxic potency of the former structural isomer (HL^3). All other investigated proligands did not reach IC$_{50}$ in the investigated range of concentrations up to 100 μM. The complexes **1, 2, 3, 5** and **6** showed IC$_{50}$ values up to 35 μM. The highest cytotoxic effect was observed for **5** in LS174 with IC$_{50}$ = 13.7 ± 0.5 μM. This effect was slightly superior to that of reference compound cisplatin (IC$_{50}$ = 22.4 ± 7.2 μM). The complexes **3** and **6** were most active in A549 cells with IC$_{50}$ values of 20.3 ± 1.8 μM and 23.2 ± 1.1 μM, respectively, and in MDA-MB-453 with IC$_{50}$ values of 30.8 ± 1.1 μM (a 2.4-fold increase of activity over that of the proligand) and 18.9 ± 1.1 μM (a 4.7-fold increase), respectively, which is comparable with the IC$_{50}$ value for cisplatin as a positive control (26.2 ± 5.4 μM and 13.5 ± 2.6, respectively). Therefore, A549 cells were chosen as a cell model for further investigation of the mechanism of the antiproliferative action of **3** and **6** (vide infra). Regretably, the complexes **1–6** did not show any selectivity for cancer cells. In contrast, complexes **3** and **4** showed a two to three times higher antiproliferative effect in normal BEAS-2B cells.

Taking into account the IC$_{50}$ values for proligands HL^1–HL^6 and their copper(II) complexes **1–6** in A549 and MDA-MB-453
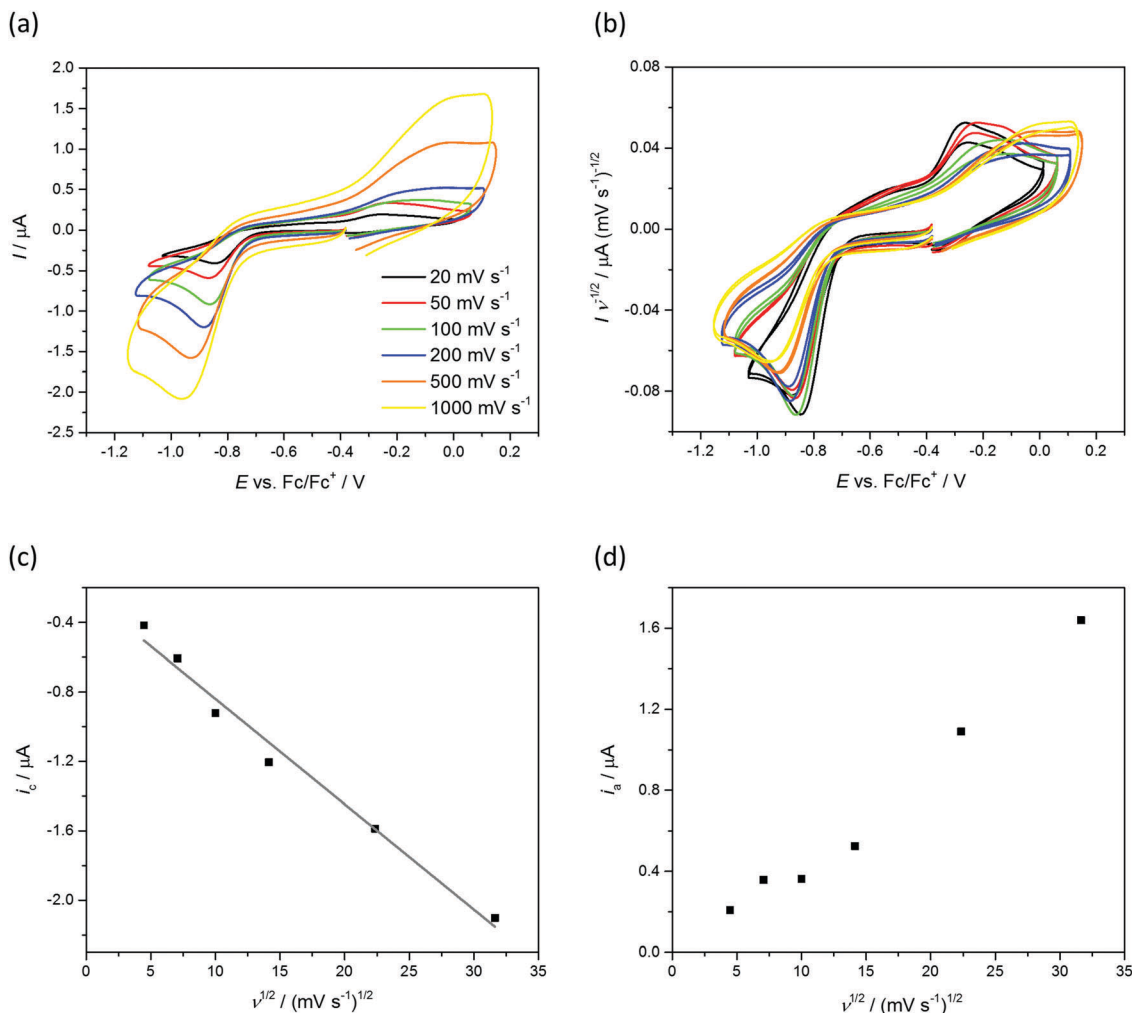

Fig. 6 The cyclic voltammograms of **4** (black trace), **5** (red trace) and **6** (green trace) in DMSO/nBu$_4$NPF$_6$ at scan rate of 100 mV s^{-1}.

Fig. 7 The cyclic voltammograms of **6** in DMSO/nBu$_4$NPF$_6$ at different scan rates: (a) $I = f(E)$ and (b) $I \cdot \nu^{-1/2} = f(E)$, as well as the dependence of the (c) cathodic and (d) anodic peak current on the square root of the scan rate.

cell lines, complex formation with copper(II) increased the cytotoxic potency of all investigated proligands. The attachment of a methyl or phenyl group at the terminal N atom of the thiosemicarbazide moiety slightly increased the cytotoxic potency of the complexes. This increased in the following rank order **1** ≈ **2** < **3** and **4** < **5** < **6** in the A549 cell line. In the MDA-MB-453 cell line the attachment of bulky groups increases cytotoxicity in the following order **4** < **5** < **6**, while in the case of complexes **1**–**3** enhancement of cytotoxicity was not observed.

Cell cycle analysis. The mechanism of cell growth inhibition by complexes **3** and **6** was investigated *via* analysis of cell cycle perturbations and apoptosis induction in A549 cells by flow cytometry. The cell cycle analysis was performed after 24 h of treatment at three different drug concentrations IC$_{50}$, 1.5IC$_{50}$, and 2IC$_{50}$ (Fig. 8). Complex **3** decreased the percent of cells in the G1 phase and increased the number of cells in S and G2 phases at all three concentrations, without any change in the population of the Sub-G1 phase (cells with fragmented DNA). Strong detachment of cells was revealed after treatment with

higher concentrations (1.5IC$_{50}$ and 2IC$_{50}$) of **3**. Treatment with **6** did not induce any morphological changes. The decrease of the percent of cells in the G1 phase and the increase of the percent of cells in S and G2 phases were similar to those observed for **3**. The cisplatin as a reference compound induced an increase of the percent of cells in the Sub-G1 phase (up to 30% with 2IC$_{50}$ concentration), and a decrease of the percent of cells in G1 and G2 phases, in accordance with the literature data.[59,60] The data of the cell cycle analysis point to the likely different mechanism of action of investigated complexes **3** and **6** compared to cisplatin in A549 cells.

Overall, both isomers revealed similar effects on the cell cycle in A549 cells after 24 h incubation. For comparison, copper(II) complexes with 8-hydroxyquinoline-2-carboxaldehyde thiosemicarbazones revealed dose-dependent cell growth inhibition, S-phase cell cycle arrest and apoptosis of cisplatin-resistant SK-N-DZ neuroblastoma cells.[61] Other closely related copper(II) compounds were found to cause cell cycle arrest in the G2/M phase in human non-small cell lung cancer (NSCLC) cell line A549.[8a]

Table 2 Results of MTT assay for proligands **HL$^{1-6}$** and copper(II) complexes **1–6** after 48 h treatment

IC$_{50}$ ± SD [μM]				
Cell line				
Compound	A549	MDA-MB-453	LS174	BEAS-2B
HL^1	>100	>100	>100	>100
HL^2	>100	>100	>100	>100
HL^3	>100	74.0 ± 1.8	33.6 ± 2.3	33.8 ± 1.1
HL^4	>100	>100	>100	>100
HL^5	>100	>100	>100	>100
HL^6	>100	87.9 ± 2.7	42.6 ± 1.3	56.0 ± 4.6
1	28.4 ± 2.8	30.7 ± 1.2	33.6 ± 2.8	21.5 ± 1.6
2	30.5 ± 2.6	30.0 ± 0.7	23.7 ± 0.5	24.8 ± 1.5
3	20.3 ± 1.8	30.8 ± 1.1	33.4 ± 1.0	10.2 ± 0.7
4	66.4 ± 2.5	51.4 ± 4.6	44.2 ± 2.4	22.7 ± 1.7
5	33.8 ± 2.8	29.0 ± 1.3	13.7 ± 0.5	26.2 ± 1.8
6	23.2 ± 1.1	18.9 ± 1.1	35.0 ± 1.3	14.0 ± 1.4
Cisplatin*	26.2 ± 5.4	13.5 ± 2.6	22.4 ± 7.2	14.2 ± 1.4

The sign (>) indicates that the IC$_{50}$ value was not reached in the examined range of concentrations (the sign is in front of the maximum value of the concentration in the used range of concentrations). * Results published previously.[58]

Further investigation of cell cycle perturbations induced by the investigated complexes after prolonged drug exposure (48 h) (Fig. 9) showed an increase of the percent of cells in the Sub-G phase to 19% for **3** and 33% for **6** compared to the control (only 3.3%).

Obviously, the decrease of the percent of cells in the G1 phase and the accumulation of cells in S and G2 phases after 24 h treatment, which continued after 48 h treatment, induced cell demise.

Flow-cytometric analysis of apoptotic potential by annexin-V-FITC/PI. In order to investigate the nature of cell death induced by **3** and **6**, annexin-V-FITC and propidium iodide (PI) staining was performed. Apoptotic cell death, in most cell types, is accompanied by a change in plasma membrane structure by surface exposure of phospholipid phosphatidylserine (PS), while the membrane integrity is retained.[62,71] Surface exposed PS can be detected by protein annexin-V.[71] To distinguish apoptotic cells from nonapoptotic cells, annexin-V staining is usually combined with cell-impermeable dyes, such as propidium
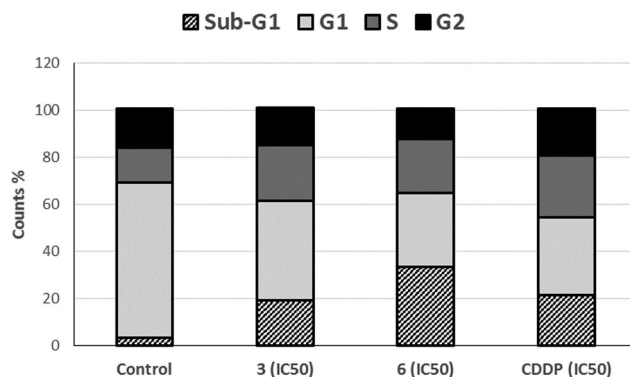

Fig. 9 Cell cycle analysis of A549 cancer cells after 48 h of exposure to investigated complexes **3** and **6** and cisplatin (CDDP). The concentrations of agent used for treatment were concentrations corresponding to IC$_{50}$.

iodide (PI). The incubation of A549 cells with **3** and **6** for 24 h and IC$_{50}$ concentrations did not induce PS externalisation (Fig. 10 and Fig. S18, ESI†).

The majority of cells treated with **3**, **6** and cisplatin for 24 h preserved cell membrane integrity as over 80% of cells did stain neither with annexin-V-FITC nor with PI. Only in the case of cisplatin a higher percent of cells with damaged membranes was detected (18% compared to control 3%). These results indicate that after 24 h incubation with **3** and **6** at concentrations equivalent to IC$_{50}$, A549 cells remained alive.

As pointed out in cell cycle analysis as well, upon cell collection after the treatment with **3** it was observed that the cells became round and detached from the surface on a large scale. Upon treatment with an IC$_{50}$ concentration of **3**, approximately 10% of cells became round and detached, while at a 1.5IC$_{50}$ concentration of the drug all cells became round and detached. Treatment with **6** at IC$_{50}$ and 1.5IC$_{50}$ concentrations for 24 h did not induce any morphological changes. Hence, further investigations with a higher concentration (2IC$_{50}$) of the investigated agent were conducted. The results showed the same trend of morphological changes without PS externalisation (Fig. S19, ESI†). Extended incubation to 48 h showed similar results (Fig. S20, ESI†). The majority of the cells treated with **3** and **6** preserved cell membrane integrity with no PS
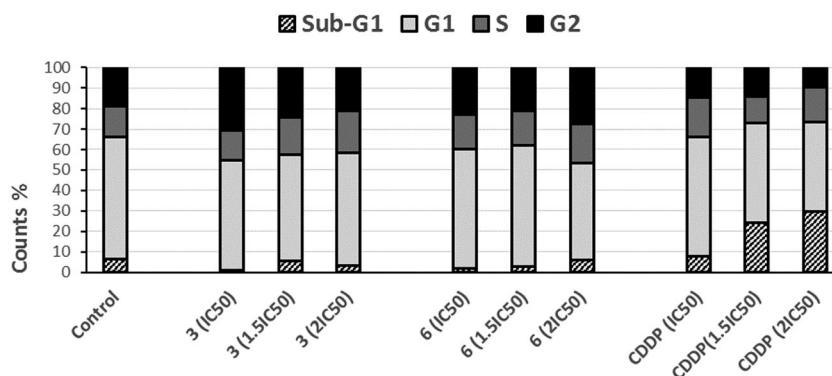

Fig. 8 Cell cycle analysis of A549 cancer cells after 24 h of exposure to **3** and **6** and cisplatin (CDDP). The concentrations of agents used for treatment were concentrations corresponding to IC$_{50}$, 1.5IC$_{50}$ and 2IC$_{50}$. The flow cytometric analysis was carried out after PI staining.
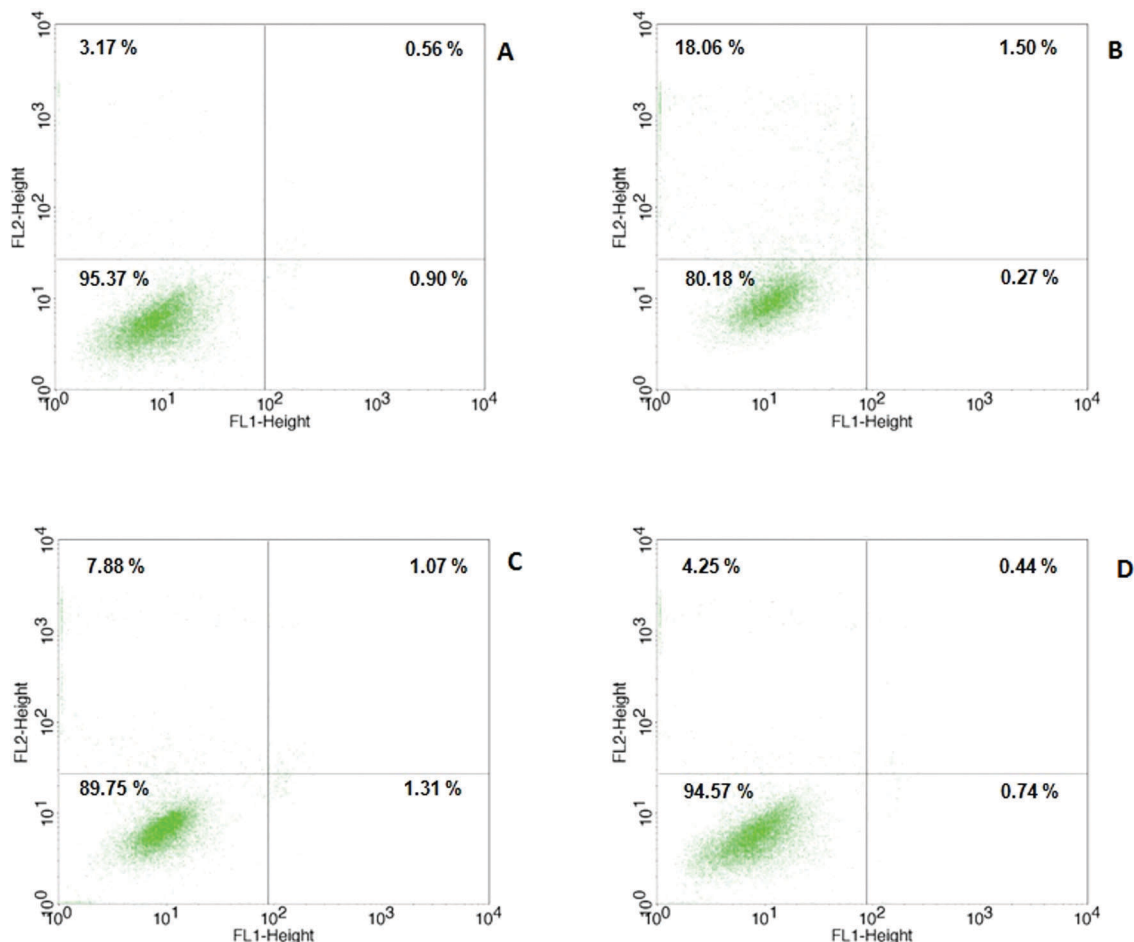
Fig. 10 The presented dot plots combining annexin-V-FITC (FL1-height) and PI (FL2-height) fluorescence show the quantification of apoptosis in A549 cells treated with cisplatin (B), **3** (C) and **6** (D) as well as untreated cells (A). The cells were treated with IC_{50} concentrations of compounds for 24 h. The viable cell population is in the lower left quadrant (annexin-V−FITC/PI−), the early apoptotic cells are in the lower right quadrant (annexin-V+/PI−), the late apoptotic cells are in the upper right quadrant (annexin-V+/PI+), and the dead cells are in the upper left quadrant (annexin-V−FITC/PI+).

externalisation. The percent of cells with damaged membranes (dead cells) increased to about 12%, as compared to control 3%, while cisplatin was able to induce an increase of the percent of apoptotic cells. Taking into account that apoptosis is a stochastic event with variable induction and execution kinetics,[62] further analysis with variations in time and concentrations of treatment, as well as introduction of other methods, is required to determine whether **3** and **6** have apoptotic potential.

Results of morphological analysis of cell death. Fluorescence microscopy after acridine orange/ethidium bromide (AO/EB) staining was used to analyse morphological changes induced by the investigated complexes. AO (green) is a vital dye, which stains both live and dead cells, while EB (orange to red) only
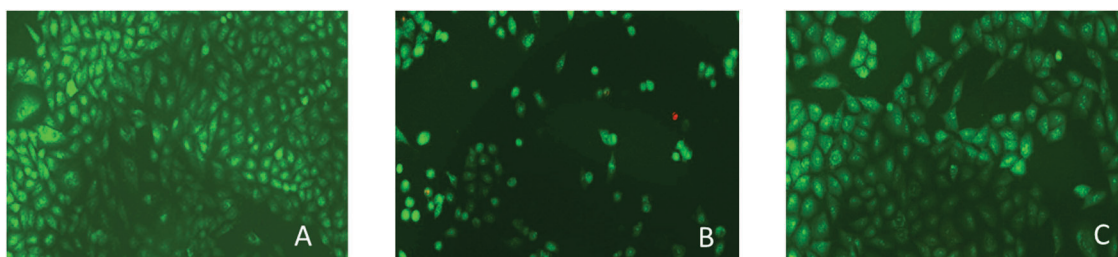
Fig. 11 Fluorescent micrographs presenting A549 cells: (A) the untreated cells used as a control and (B) cells treated with **3** and (C) cells treated with **6** for 24 h with concentrations corresponding to $2IC_{50}$. Cells stained with ethidium bromide (EB) and acridine orange (AO) were analysed with a fluorescent microscope (Axio Observer Z1) by using AxioVision imaging software (Carl Zeiss MicroImaging GmbH). AO (green) is a vital dye, which stains both live and dead cells. EB (orange to red) only stains cells that have lost membrane integrity.

stains cells that have lost membrane integrity.[63] The micro-photographs of A549 cells stained by AO/EB, following 24 h treatment with **3** and **6**, are displayed in Fig. 11. Control cells (non-treated cells) are dense, light-green coloured and elongated with a spindle-shape (Fig. 11A). After 24 h treatment, with a $2IC_{50}$ concentration of **3**, cells started to lose their normal morphology and became rounded, and reduced in size, with still intact cell membranes, since cells incorporated only AO (green fluorescence). Several early apoptotic cells with condensed or fragmented chromatin were spotted. The number of cells was markedly reduced compared to the control, as many of them detached (Fig. 11B). At the same time complex **6** after 24 h treatment at a $2IC_{50}$ concentration induced only a slight reduction of the number of cells compared to the control, without noticeable morphological changes (Fig. 11C). These results are in compliance with the results of apoptotic potential by annexin-V-FITC and PI staining, as well as flow cytometric analysis.

Whether this behaviour is due to the presence of dichloro-acetate in investigated complexes, should be clarified in our future investigations, which will require the synthesis of analogous copper(II) complexes without dichloroacetate.

3 Conclusions

Six methyl imidazole-derived thiosemicarbazones and their corresponding copper(II) complexes were synthesised and characterised by NMR, IR, UV-vis spectroscopy, ESI-MS spectrometry, X-ray crystallography and elemental analysis. According to NMR spectroscopic data, all proligands exist as geometric Z and E isomers in a 1:1 molar ratio in DMSO solution except $\mathbf{HL^2}$, for which the Z isomer is favoured (79%). Due to the fast proton exchange, acid–base tautomerism of the imidazole ring was observed. At higher pH values thione/thiol tautomerism of the thiosemicarbazide moiety occurred in accordance with solution equilibrium studies of other related thiosemicarbazones. In the investigated pH range 2–12, two proton dissociation constants were attributed to two proton donors, namely imidazole $N^{2'}H$ and hydrazine $N^{4'}H$ groups. At physiological pH the proligands are present in neutral **HL** form.

All thiosemicarbazone ligands are coordinated to copper(II) in a tridentate NNS manner in their neutral form and together with dichloroacetate as a co-ligand form cationic complexes $[Cu(\mathbf{HL^{1-6}})(CHCl_2CO_2)]^+$ (in **1–6**), which are counterbalanced by another dichloroacetate anion building neutral ionic complexes, which are isolated in the solid state. Copper(II) adopts distorted square-planar (in **1**, **4** and **5**) or square-pyramidal (in **2**, **3** and **6**) coordination geometry. According to electrochemical studies the complexes **1–6** can undergo redox processes in a biologically accessible window (–0.4 to +0.8 V $vs.$ NHE).

The cell growth inhibition study showed that introduction of a phenyl substituent at the terminal N atom of the thiosemi-carbazide moiety of the proligands $\mathbf{HL^3}$ and $\mathbf{HL^6}$ enhances their antiproliferative efficiency in LS174 and MDA-MB-453 cell lines when compared to other proligands. In addition, the proligand

$\mathbf{HL^3}$ with the methyl group at position 2 of the imidazole ring exhibited slightly better potency compared to its structural isomer $\mathbf{HL^6}$ with the methyl group at position 5. Coordination to copper(II) induced enhancement of the cytotoxic effect of all proligands in all investigated cell lines. In particular, the complexes **3** and **6**, both with phenyl substituted ligands at the terminal N atom, revealed a 2.4- and 4.7-fold increase of antiproliferative activity compared to their parent proligands in the MDA-MB-453 cell line. Overall, according to the IC_{50} values, the following rank orders of cytotoxic efficiency of the proligands $\mathbf{HL^{1-6}}$ and their copper(II) complexes **1–6** could be established: $\mathbf{HL^1} \approx \mathbf{HL^2} \approx \mathbf{HL^3} < \mathbf{1} \approx \mathbf{2} < \mathbf{3}$ and $\mathbf{HL^4} \approx \mathbf{HL^5} \approx \mathbf{HL^6} < \mathbf{4} < \mathbf{5} < \mathbf{6}$ in the A549 cell line, and $\mathbf{HL^1} \approx \mathbf{HL^2} < \mathbf{HL^3} < \mathbf{1} \approx \mathbf{2} \approx \mathbf{3}$ and $\mathbf{HL^4} \approx \mathbf{HL^5} < \mathbf{HL^6} < \mathbf{4} < \mathbf{5} < \mathbf{6}$ in the MDA-MB-453 cell line. The highest activity was observed in the cell line LS174 for **5** (IC_{50} =13.7 $\pm$ 0.5 μM). This is slightly better than for cisplatin as a positive control (IC_{50} = 22.4 $\pm$ 7.2 μM). All investigated complexes showed poor selectivity to cancer cells when compared to their activity against normal human bronchial epithelial cells (BEAS-2B) and were in this respect similar to cisplatin.

Even though **3** and **6** showed IC_{50} values (20 μM and 23 μM, respectively) in A549 cells comparable to that for cisplatin (26 μM), indicating similar cell growth inhibiting potential, further insight into their mechanism of antiproliferative activity revealed that these complexes probably act in a different way than cisplatin. MTT assay determines the number of viable cells via the measurement of the activity of mitochondrial enzymes present in metabolically active cells. Therefore, it cannot distinguish between cytostatic and cytocidal effects.[69] Our investigation of cell cycle, apoptotic potential and morphological analysis of changes induced by **3** and **6** pointed to cytostatic rather than cytotoxic effects of investigated complexes with an important anti-adhesion effect of complex **3** on A549 cells. Even though cell cycle analysis and annexin-V-FITC/PI staining indicate that there are no major differences in the activity among these two complexes regardless of the structural differences, the fluorescent microscopy analysis revealed considerable differences in the activity of these two isomeric complexes at least in the "time window" of action/where the morphological changes take place. Further investigations into the contribution of dichloroacetate to the observed biological response of the cells to complexes **3** and **6** are underway in our laboratory and will be reported in due course.

4 Experimental section

4.1 Materials and methods

2-Methyl-1H-imidazole-4-carboxaldehyde, and 4-methyl-1H-imidazole-5-carboxaldehyde were purchased from Acros Organics. Thiosemicarbazide, 4-methylthiosemicarbazide and 4-phenylthio-semicarbazide, dichloroacetic acid, copper(II) basic carbonate, KOH, KCl, 4-(2-hydroxyethyl)-1-piperazineethane-sulfonic acid (HEPES), and ethylenediaminetetraacetic acid (EDTA) were purchased from Sigma Aldrich. Elemental analysis of $\mathbf{HL^{1-6}}$ was performed on a Carlo Erba microanalyser at the Micro-analytical Laboratory of the University of Vienna. Electrospray

ionisation mass spectrometry measurements were carried out on a Bruker Esquire 3000 instrument (Bruker Daltonic, Bremen, Germany) at the Mass Spectrometry Centre of the Faculty of Chemistry of the University of Vienna. UV-vis spectra were measured on a Perkin-Elmer Lambda 650 spectrophotometer in the range 900–210 nm. The samples were prepared by dissolving the compounds in MeOH or DMF (for complexes 2 and 3). Infrared spectra were recorded on Perkin-Elmer FT-IR 2000 instrument (4000–400 cm^{-1}) using an ATR unit or Bruker Vertex 70 FT-IR spectrometer. NMR spectra were acquired on a Bruker Avance III 500 MHz FT NMR spectrometer. All samples were prepared by dissolving the compounds in (CD$_3$)$_2$SO.

4.2 Synthesis of proligands and copper(II) complexes

(E/Z)-2-((2-Methyl-1H-imidazol-4-yl)methylene)hydrazine-1-carbothioamide (HL^1·0.65H$_2$O). A mixture of 2-methyl-1H-imidazole-4-carboxaldehyde (1.10 g, 10 mmol) and thiosemicarbazide (0.91 g, 10 mmol) in EtOH (10 mL) was refluxed for 2 h and then cooled down to 0 °C. The pale yellow precipitate was filtered off, washed with cold absolute EtOH (2 mL) and dried *in vacuo* overnight. Yield: 1.75 g, 90%. Anal. calcd for C$_6$H$_9$N$_5$S·0.65H$_2$O (*M*$_r$ 194.95), %: C, 36.97; H, 5.33; N, 35.92; S, 16.45. Found, %: C, 36.99; H, 5.33; N, 35.50; S, 16.90. ^{1}H NMR (500.10 MHz, (CD$_3$)$_2$SO, 25 °C) *Z* isomer: δ 11.94 (s, 1H, **HN$^{1'}$**), 11.34 (s, 1H, **HN$^{4'}$**), 8.17 (s, 1H, **H$_a$N$^{5'}$**), 7.86 (s, 1H, **HC^5**), 7.82 (s, 1H, **H$_b$N$^{5'}$**), 7.21 (s, 1H, **HC^2**), 2.30 (s, 3H, **H$_3$C^4**) ppm. *E* isomer: δ 12.97 (s, 1H, **HN$^{4'}$**), 12.50 (s, 1H, **HN$^{1'}$**), 8.17 (s, 1H, **H$_a$N$^{5'}$**), 7.79 (s, 1H, **H$_b$N$^{5'}$**), 7.55 (s, 1H, **HC^5**), 7.12 (s, 1H, **HC^2**), 2.38 (s, 3H, **H$_3$C^4**) ppm. ^{13}C{^{1}H} NMR (125.76 MHz, (CD$_3$)$_2$SO, 25 °C) *Z* isomer: δ 177.92 (C^6), 146.92 (C^1), 133.48 (C^5), 129.93 (C^3), 128.91 (C^2), 14.27 (C^4) ppm. *E* isomer: δ 178.10 (C^6), 145.76 (C^1), 135.65 (C^3), 131.79 (C^5), 122.07 (C^2), 14.39 (C^4) ppm. ESI-MS in MeOH (positive): *m/z* 184 ([**HL^1** + H]$^+$), 206 ([**HL^1** + Na]$^+$). ESI-MS in MeOH (negative): *m/z* 182 ([**L^1**]$^-$). UV-vis in MeOH, λ, nm (ε, M^{-1} cm^{-1}): 306 (29 898), 315 (29 614). IR (selected bands), $\tilde{\nu}$, cm^{-1}: 3553 (NH$_2$), 3155 (Ar–H), 1613 (C=N), 785 (C–S).

(E/Z)-N-Methyl-2-((2-methyl-1H-imidazol-4-yl)methylene)-hydrazine-1-carbothioamide (HL^2·0.6H$_2$O). To a solution of 2-methyl-1H-imidazole-4-carboxaldehyde (1.10 g, 10 mmol) in dry ethanol (10 mL) 4-methylthiosemicarbazide (1.05 g, 10 mmol) in dry ethanol (10 mL) was added. The reaction mixture was refluxed for 2 h and then cooled down to 0 °C. The pale yellow precipitate was filtered off, washed with cold ethanol (2 mL) and dried *in vacuo* overnight. Yield: 1.9 g, 92%. Anal. calcd for C$_7$H$_{11}$N$_5$S·0.6H$_2$O (*M*$_r$ 208.07), %: C, 40.41; H, 5.91; N, 33.66; S, 15.41. Found, %: C, 40.06; H, 5.88; N, 33.29; S, 15.33. ^{1}H NMR (500 MHz, (CD$_3$)$_2$SO, 25 °C) *Z* isomer: δ 11.99 (s, 1H, HN$^{1'}$), 11.36 (s, 1H, HN$^{4'}$), 8.26 (m, 1H, HN$^{5'}$), 7.87 (s, 1H, HC^5), 7.24 (s, 1H, HC^2), 3.03 (d, 3H, **H$_3$C^7**), 2.33 (s, 3H, **H$_3$ C^4**); *E* isomer, δ, ppm: 13.01 (s, 1H, HN$^{4'}$), 12.49 (s, 1H, HN$^{1'}$), 8.46 (m, 1H, HN$^{5'}$), 7.54 (s, 1H, HC^5), 7.11 (s, 1H, HC^5), 2.97 (d, 3H, **H$_3$C^7**), 2.38 (s, 3H, **H$_3$C^4**) ppm. ^{13}C{^{1}H} NMR (125.76 MHz, (CD$_3$)$_2$SO, 25 °C) *Z* isomer: δ 177.81 (C^6), 146.99 (C^1), 133.91 (C^5), 130.96 (C^3), 126.43 (C^2), 31.00 (C^7), 14.43 (C^4) ppm. *E* isomer: δ 177.88 (C^6), 145.74 (C^1), 135.67 (C^3), 131.10 (C^5), 121.86 (C^2), 31.26 (C^7), 14.34 (C^4) ppm. ESI-MS in MeOH

(positive): *m/z* 198 ([**HL^2** + H]$^+$), 220 ([**HL^2** + Na]$^+$). ESI-MS in MeOH (negative): *m/z* 196 ([**L^2**]$^-$). UV-vis in MeOH, λ, nm (ε, M^{-1} cm^{-1}): 306 (32 678), 316 (32 205). IR (selected bands), $\tilde{\nu}$, cm^{-1}: 3380 (NH$_2$), 3152 (Ar–H), 1627 (C=N), 771 (C–S).

(E/Z)-2-((2-Methyl-1H-imidazol-4-yl)methylene)-N-phenyl-hydrazine-1-carbothioamide (HL^3·H$_2$O). A mixture of 2-methyl-1H-imidazole-4-carboxaldehyde (1.1 g, 10 mmol) and 4-phenyl-thiosemicarbazide (1.67 g, 10 mmol) in absolute EtOH (10 mL) was refluxed for 2 h and then cooled down to 0 °C. The pale yellow precipitate was filtered off, washed with cold ethanol (2 mL) and dried *in vacuo* overnight. Yield: 2.60 g, 94%. Anal. calcd for C$_{12}$H$_{13}$N$_5$S·H$_2$O (*M*$_r$ 277.35), %: C, 51.97; H, 5.45; N, 25.25; S, 11.56. Found, %: C, 52.10; H, 5.40; N, 24.97; S, 11.36. ^{1}H NMR (500.10 MHz, (CD$_3$)$_2$SO, 25 °C) *Z* isomer: δ 12.19 (s, 1H, **HN$^{4'}$**), 11.79 (s, 1H, **HN$^{1'}$**), 9.94 (s, 1H, **HN$^{1'}$**), 7.98 (s, 1H, **HC^5**), 7.60 (s, 1H, **HC^8 or HC^{10}**), 7.58 (s, 1H, **HC^8 or HC^{10}**), 7.39 (m, 2H, **HC^9 and HC^{11}**), 7.21 (t, 1H, **HC^{10}**), 2.33 (s, 3H, **H$_3$C^4**) ppm; *E* isomer: δ 13.39 (s, 1H, **HN$^{4'}$**), 12.56 (s, 1H, **HN$^{1'}$**), 10.16 (s, 1H, **HN$^{5'}$**), 7.66 (s, 1H, **HC^8 or HC^{10}**), 7,64 (s, 1H, **HC^8 or HC^{10}**), 7.25 (s, 1H, **HC^5**), 7.33 (m, 2H, **HC^9 and HC^{11}**), 7.15 (t, 1H, **HC^{10}**), 2.4 (s, 3H, **H$_3$C^4**) ppm. ^{13}C{^{1}H} NMR (125.76 MHz, (CD$_3$)$_2$SO, 25 °C), *Z* isomer: δ 175.68 (C^6), 139.35 (C^7), 128.74 (C^9), 128.74 (C^{11}), 125.86 (C^8), 125.86 (C^{12}), 14.55 (C^4) ppm. *E* isomer: δ 175.68 (C^6), 145.91 (C^1), 139.54 (C^7), 135.47 (C^3)132.02 (C^5), 128.52 (C^9), 128.52 (C^{11}), 125.36 (C^{10}), 125.18 (C^8), 125.18 (C^{12}), 122.5 (C^2), 14.30 (C^4) ppm. ESI-MS in MeOH (positive): *m/z* 260 ([**HL^3** + H]$^+$) 282 ([**HL^3** + Na]$^+$). ESI-MS in MeOH (negative): *m/z* 258 ([**L^3**]$^-$). UV-vis in MeOH, λ, nm (ε, M^{-1} cm^{-1}): 208 (16 198), 317 (29 092). IR (selected bands), $\tilde{\nu}$, cm^{-1}: 3488 (NH$_2$), 3133 (Ar–H), 1622 (C=N), 746 (C–S).

(E/Z)-2-((5-Methyl-1H-imidazol-4-yl)methylene)hydrazine-1-carbothioamide (HL^4). A mixture of 5-methyl-1H-imidazole-4-carboxaldehyde (1.1 g, 10 mmol) and thiosemicarbazide (0.91 g, 10 mmol) in dry ethanol (10 mL) was refluxed for 2 h and cooled down to 0 °C. The pale-yellow precipitate was filtered off, washed with cold absolute ethanol (2 mL) and dried *in vacuo* overnight. Yield 1.7 g, 93%. Anal. calcd for C$_6$H$_9$N$_5$S (*M*$_r$ 183.24), %: C, 39.33; H, 4.95; N, 38.22; S, 17.50. Found, %: C, 39.49; H, 4.98; N, 37.78; S, 17.15. ^{1}H NMR (500.10 MHz, (CD$_3$)$_2$SO, 25 °C), *Z* isomer: δ 12.29 (s, 1H, HN$^{1'}$), 11.28 (s, 1H, HN$^{4'}$), 8.13 (s, 1H, HaN$^{5'}$), 7.89 (s, 1H, HC^5), 7.68 (s, 1H, HC^1), 2.19 (s, 3H, **H$_3$C^4**) ppm. *E* isomer: δ 13.11 (s, 1H, HN$^{4'}$), 11.28 (s, 1H, HN$^{1'}$), 8.18 (s, 1H, HaN$^{5'}$), 7.98 (s, 1H, HC^1), 7.76 (s, 1H, HbN^5), 7.21 (s, 1H, HC^5), 2.36 (s, 3H, **H$_3$C^4**) ppm. ^{13}C{^{1}H} NMR (125.76 MHz, (CD$_3$)$_2$SO, 25 °C) *Z* isomer: δ 177.81 (C^6), 137.48 (C^1), 135.28 (C^5), 13.20 (C^4) ppm. *E* isomer: δ 178.05 (C^6), 131.43 (C^1), 130.82 (C^5), 9.50 (C^4) ppm. ESI-MS in MeOH (positive): *m/z* 184 ([**HL^4** + H]$^+$) 206 ([**HL^4** + Na]$^+$). ESI-MS in MeOH (negative): *m/z* 182 ([**L^4**]$^-$). UV-vis in MeOH, λ, nm (ε, M^{-1} cm^{-1}): 208 (9607), 306 (28 298), 316 (27 558). IR (ATR, selected bands), $\tilde{\nu}$, cm^{-1}: 3388 (NH$_2$), 3149 (Ar–H), 1593 (C=N), 710 (C–S).

(E/Z)-N-Methyl-2-((5-methyl-1H-imidazol-4-yl)methylene)-hydrazine-1-carbothioamide (HL^5). A mixture of 5-methyl-1H-imidazole-4-carboxaldehyde (1.1 g, 10 mmol) and 4-methyl-3-thiosemicarbazide (1.05 g, 10 mmol) in absolute ethanol

(10 mL) was refluxed for 2 h and cooled down to 0 °C. The pale yellow precipitate was filtered off, washed with cold absolute ethanol (2 mL) and dried *in vacuo* overnight. Yield: 1.8 g, 91%. Anal. calcd for $C_7H_{11}N_5S$ (M_r 197.26), %: C, 42.62; H, 5.62; N, 35.50; S, 16.26. Found, %: C, 42.71; H, 5.65; N, 35.21; S, 16.23. ^{1}H NMR (500.10 MHz, $(CD_3)_2SO$, 25 °C), *Z* isomer: δ 12.21 (s, 1H, $HN^{1'}$), 11.31 (s, 1H, $HN^{4'}$), 8.22 (m, 1H, $HN^{5'}$), 7.90 (s, 1H, HC^5), 7.71 (s, 1H, HC^1), 3.03 (d, 3H, H_3C^7), 2.24 (s, 3H, H_3C^4) ppm. *E* isomer: δ 13.17 (s, 1H, $HN^{4'}$), 12.66 (s, 1H, $HN^{1'}$), 8.43 (s, 1H, $HN^{5'}$), 8.00 (s, 1H, HC^1), 7.20 (s, 1H, HC^5), 2.98 (d, 3H, H_3C^7), 2.38 (s, 3H, H_3C^4) ppm. ^{13}C{^{1}H} NMR (125.76 MHz, $(CD_3)_2SO$, 25 °C), *Z* isomer: δ 177.79 (C^6), 136.74 (C^1), 135.20 (C^5), 131.58 (C^3), 31.00 (C^7), 12.37 (C^4) ppm. *E* isomer: δ 177.90 (C^6), 130.13 (C^5), 131.82 (C^3), 31.29 (C^7), 9.52 (C^4) ppm. ESI-MS in MeOH (positive): *m/z* 198 ($[HL^5 +$ H]$^+$), 220 ($[HL^5 + Na]^+$). ESI-MS in MeOH (negative): *m/z* 196 ($[L^5]^-$). UV-vis in MeOH, λ, nm (ε, M^{-1} cm^{-1}): 208 (9694), 308 (25 370), 318 (24 326). IR (selected bands), $\tilde{\nu}$, cm^{-1}: 3151 (Ar–H), 1620 (C=N), 755 (C–S).

(*E*/*Z*)-2-((5-Methyl-1*H*-imidazol-4-yl)methylene)-*N*-phenyl-hydrazine-1-carbothioamide (HL⁶). A mixture of 5-methyl-1*H*-imidazole-4-carboxaldehyde (1.10 g, 10 mmol) and 4-phenyl-thiosemicarbazide (1.67 g, 10 mmol) in dry EtOH (10 mL) was refluxed for 2 h and then cooled down to 0 °C. The pale yellow precipitate was filtered off, washed with cold EtOH (2 mL) and dried *in vacuo* overnight. Yield: 2.4 g, 93%. Anal. calcd for $C_{12}H_{13}N_5S$ (M_r 259.33), %: C, 55.58; H, 5.05; N, 27.01; S, 12.36. Found, %: C, 55.46; H, 5.06; N, 26.69; S, 12.13. ^{1}H NMR (500 MHz, $(CD_3)_2SO$, 25 °C), *Z* isomer: δ 12.42 (s, 1H, $HN^{1'}$), 11.72 (s, 1H, $HN^{4'}$), 9.93 (s, 1H, $HN^{5'}$), 8.11 (s, 1H, HC^5), 7.78 (s, 1H, HC^1), 7.62 (d, 2H, HC^8 and HC^{12}), 7.41–7.36 (m, 2H, HC^9 and HC^{12}), 7.21 (t, 1H, HC^{10}), 2.26 (s, 3H, H_3C^4) ppm. *E* isomer: δ 13.50 (s, 1H, $HN^{4'}$), 12.74 (s, 1H, $HN^{1'}$), 10.14 (s, 1H, $HN^{5'}$), 7.95 (s, 1H, HC^1), 7.66 (d, 2H, HC^8 and HC^{12}), 7.36–7.31 (m, 3H, HC^9, HC^{12} and HC^5), 7.16 (t, 3H, HC^{10}), 2.41 (s, 3H, H_3C^4). ^{13}C{^{1}H} NMR (125.76 MHz, $(CD_3)_2SO$, 25 °C), *Z* isomer: δ 175.41 (C^6), 139.32 (C^7), 137.16 (C^1), 128.71 (C^9 and C^{11}), 125.64 (C^{10}), 125.43 (C^8 and C^{12}), 12.60 (C^4) ppm. *E* isomer: δ 175.70 (C^6), 139.53 (C^7), 135.46 (C^1), 131.82 (C^3), 131.01 (C^5), 132.32 (C^2), 131.72 (C^3), 128.49 (C^9 and C^{11}), 125.35 (C^{10}), 125.20 (C^8 and C^{12}), 9.57 (C^4) ppm. ESI-MS in MeOH (positive): *m/z* 260 ($[HL^6 +$ H]$^+$), 282 ($[HL^6 + Na]^+$). ESI-MS in MeOH (negative): *m/z* 258 ($[L^6]^-$). UV-vis in MeOH, λ, nm (ε, M^{-1} cm^{-1}): 207 (18 839), 318 (31 074). IR (selected bands), $\tilde{\nu}$, cm^{-1}: 3321 (NH₂), 3117 (Ar–H), 1611 (C=N), 740 (C–S).

[Cu(HL¹)(CHCl₂CO₂)]CHCl₂CO₂ (1). To a solution of HL¹ (0.19 g, 1.0 mmol) in ethanol (15 mL) was added dropwise under stirring a solution of $Cu_2(OH)_2CO_3$ (0.12 g, 0.5 mmol) and dichloroacetic acid (0.19 g, 1.0 mmol) in water (15 mL). The reaction mixture was refluxed at 70 °C for 30 min, cooled down, and allowed to stand for 3–4 days at room temperature. Slow solvent evaporation resulted in precipitation of a green product, which was filtered off, washed with ethanol (2 × 2 mL) and dried *in vacuo*. X-ray diffraction quality single crystals of **1** were obtained by re-crystallisation in ethanol. Yield: 0.44 g, 88%. ESI-MS in MeOH (positive): *m/z* 245 ($[Cu^{II}(L^1)]^+$), 619 ($[Cu_2^{II}(L^1)_2(CHCl_2CO_2)]^+$).

ESI-MS in MeOH (negative): *m/z* 373 ($[Cu^{II}(L^1–H)(CHCl_2CO_2)]^-$), 617 ($[Cu_2^{II}(L^1–H)_2(CHCl_2CO_2)]^-$). UV-vis in MeOH, λ, nm (ε, M^{-1} cm^{-1}) 203 (8075), 282 (7276), 335 (7837), sh 363 (5100) 632 (158). IR (selected bands), $\tilde{\nu}$, cm^{-1}: 1644 (C=N), 1576 (COO$_{as}$), 1356 (COO$_s$), 701 (C–S).

[Cu(HL²)(CHCl₂CO₂)(H₂O)]CHCl₂CO₂·H₂O (2). To a solution of HL² (0.2 g, 1.0 mmol) in ethanol (15 mL) was added dropwise under stirring a solution of $Cu_2(OH)_2CO_3$ (0.12 g, 0.5 mmol) and dichloroacetic acid (0.19 g, 1.0 mmol) in water (15 mL). The reaction mixture was refluxed at 70 °C for 30 min, cooled down, and allowed to stand for 3 days at room temperature. Slow solvent evaporation resulted in precipitation of a green solid. This was filtered off, washed with ethanol (2 × 2 mL) and dried *in vacuo* overnight. X-ray diffraction quality crystals of **2** were obtained by re-crystallisation in ethanol. Yield: 0.42 g, 81%. ESI-MS in MeOH (positive): *m/z* 259 ($[Cu^{II}(L^2)]^+$), 647 ($[Cu_2^{II}(L^2)_2(CHCl_2CO_2)]^+$). ESI-MS in MeOH (negative): *m/z* 387 ($[Cu^{II}(L^2–H)(CHCl_2CO_2)]^-$), 645 ($[Cu_2^{II}(L^2–H)_2(CHCl_2CO_2)]^-$). UV-vis in DMF, λ, nm (ε, M^{-1} cm^{-1}) 293 (17 287), 353 (14 197), 587 (233). IR (selected bands), $\tilde{\nu}$, cm^{-1}: 1630 (C=N), 1570 (COO$_{as}$), 1353 (COO$_s$), 720 (C–S).

[Cu(HL³)(CHCl₂CO₂)(EtOH)]CHCl₂CO₂ (3). To a solution of HL³ (0.28 g, 1.0 mmol) in ethanol (15 mL) a solution of $Cu_2(OH)_2CO_3$ (0.12 g, 0.50 mmol) and dichloroacetic acid (0.19 g, 1.0 mmol) in water (15 mL) was added dropwise under stirring. The reaction mixture was refluxed at 70 °C for 30 min., cooled down, and allowed to stand for 3 days at room temperature. Slow solvent evaporation resulted in precipitation of a green product. This was filtered off, washed with ethanol (2 × 2 mL) and dried *in vacuo*. X-ray diffraction quality crystals of **3** were obtained by re-crystallisation in ethanol. Yield: 0.55 g, 92%. ESI-MS in MeOH (positive): *m/z* 321 ($[Cu^{II}(L^3)]^+$), 771 ($[Cu_2^{II}(L^3)_2(CHCl_2CO_2)]^+$). ESI-MS in MeOH (negative): *m/z* 449 ($[Cu^{II}(L^3–H)(CHCl_2CO_2)]^-$), 769 ($[Cu_2^{II}(L^3–H)_2(CHCl_2CO_2)]^-$). UV-vis in DMF, λ, nm (ε, M^{-1} cm^{-1}) 339 (21 862), 363 (21 442), 577 (253). IR (selected bands), $\tilde{\nu}$, cm^{-1}: 1612 (C=N), 1739 (COO$_{as}$), 1594 (COO$_{as}$), 1348 (COO$_{as}$), 1280 (COO$_s$), 698 (C–S).

[Cu(HL⁴)(CHCl₂CO₂)]CHCl₂CO₂ (4). To a solution of HL⁴ (0.18 g, 1.0 mmol) in ethanol (15 mL) a solution of $Cu_2(OH)_2CO_3$ (0.12 g, 0.5 mmol) and dichloroacetic acid (0.19 g, 1.0 mmol) in water (15 mL) was added dropwise under stirring. The reaction mixture was refluxed at 70 °C for 30 min, cooled down, and allowed to stand for 4 days at room temperature. Slow solvent evaporation generated a green product. This was filtered off, and washed with ethanol (2 × 2 mL). X-ray diffraction quality crystals of **4** were obtained by re-crystallisation in ethanol. Yield: 0.47 g, 94%. ESI-MS in MeOH (positive): *m/z* 245 ($[Cu^{II}(L^4)]^+$), 619 ($[Cu_2^{II}(L^4)_2(CHCl_2CO_2)]^+$). ESI-MS in MeOH (negative): *m/z* 373 ($[Cu^{II}(L^4–H)(CHCl_2CO_2)]^-$), 617 ($[Cu_2^{II}(L^4–H)_2(CHCl_2CO_2)]^-$). UV-vis in MeOH, λ, nm (ε, M^{-1} cm^{-1}): 202 (8119), sh 235 (4312), 283 (6874), 337 (8344), sh 367 (5245), 628 (319). IR (selected bands), $\tilde{\nu}$, cm^{-1}: 1619 (C=N), 1726 (COO$_{as}$, coordinated), 1518 (COO$_{as}$), 1354 (COO$_s$), 1248 (COO$_s$), 709 (C–S).

[Cu(HL⁵)(CHCl₂CO₂)]CHCl₂CO₂·EtOH (5). To a solution of HL⁵ (0.20 g, 1.0 mmol) in ethanol (15 mL) a solution

of $Cu_2(OH)_2CO_3$ (0.12 g, 0.5 mmol) and dichloroacetic acid (0.19 g, 1.0 mmol) in water (15 mL) was added dropwise under stirring. The reaction mixture was refluxed at 70 °C for 30 min., cooled down, and allowed to stand for 3 days at room temperature. By slow evaporation of the solvent at room temperature green product **5** was isolated. X-ray diffraction quality crystals of **5** were obtained by re-crystallisation in ethanol. Yield: 0.51 g, 91%. ESI-MS in MeOH (positive): m/z 259 ($[Cu^{II}(L^5)]^+$), 647 ($[Cu_2^{II}(L^5)_2(CHCl_2CO_2)]^+$). ESI-MS in MeOH (negative): m/z 387 ($[Cu^{II}(L^5-H)(CHCl_2CO_2)]^-$), 645 ($[Cu_2^{II}(L^5-H)_2(CHCl_2CO_2)]^-$). UV-vis in MeOH, λ, nm (ε, M^{-1} cm^{-1}): 205 (12 823), 237 (6430), 292 (10 420), 338 (13 225), sh 369 (8908), 626 (174). IR (selected bands), $\tilde{\nu}$, cm^{-1}: 1624 (C=N), 1523 (COO_{as}), 1336 (COO_s), 710 (C–S).

[Cu(HL⁶)(CHCl₂CO₂)(H₂O)]CHCl₂CO₂·EtOH (6). To a solution of **HL⁶** (0.26 g, 1.0 mmol) in ethanol (15 mL) a solution of $Cu_2(OH)_2CO_3$ (0.12 g, 0.5 mmol) and dichloroacetic acid (0.19 g, 1.0 mmol) in water (15 mL) was added dropwise under stirring. The reaction mixture was refluxed at 70 °C for 30 min., cooled down, and allowed to stand for 4 days at room temperature. Slow solvent evaporation resulted in separation of a green product. This was filtered off, washed with ethanol (2 × 2 mL) and dried *in vacuo*. X-ray diffraction quality crystals of **6** were obtained by re-crystallisation in ethanol. Yield: 0.55 g, 94%. ESI-MS in MeOH (positive): m/z 321 ($[Cu^{II}(L^6)]^+$), 771 ($[Cu_2^{II}(L^6)_2(CHCl_2CO_2)]^+$). ESI-MS in MeOH (negative): m/z 449 ($[Cu^{II}(L^6-H)(CHCl_2CO_2)]^-$), 769 ($[Cu_2^{II}(L^6-H)_2(CHCl_2CO_2)]^-$). UV-vis in MeOH, λ, nm (ε, M^{-1} cm^{-1}): 204 (23 388), 230 (16 106), 346 (19 816), 360 (18 841), sh 381 (14 783), 614 (205). IR (selected bands), $\tilde{\nu}$, cm^{-1}: 1627 (C=N), 1595 (COO_{as}), 1350 (COO_s), 692 (C–S).

4.3 Crystallographic structure determination

X-ray diffraction measurements were carried out on a Bruker X8 APEXII CCD diffractometer using graphite monochromated MoKα radiation (λ = 0.71073 Å) at 120 K. The data were processed using SAINT software.[64] The structures were solved by direct methods using Olex2[65] and refined by full-matrix least-squares on weighted F^2 with SHELXL 2015[66] using an anisotropic model for non-hydrogen atoms. All H atoms were inserted in idealised positions (d_{CH} = 0.96 Å) using the riding model with their isotropic displacement parameters fixed at 120% of their riding atom. Positional parameters of the H attached to O or N atoms were obtained from difference Fourier syntheses and verified by the geometric parameters of the corresponding hydrogen bonds. The molecular plots were obtained using the Olex2 program. The crystallographic data and refinement details are quoted in Table 3, while bond lengths and bond angles are summarised in Tables S1–S7, ESI.† CCDC – 1577585 for **1**, 1845470 for **2**, 1845471 for **3**, 1845472 for **4**, 1845473 for **5** and 1845474 for **6** contain the supplementary crystallographic data for this contribution.†

4.4 Spectrophotometric measurements (solution equilibrium studies)

A Hewlett Packard 8452A diode array spectrophotometer was used to record the UV-vis spectra in the interval 200–800 nm. The path length was 1 cm. Protonation constants ($\beta(H_iL)$) of the ligands **HL¹** and **HL⁴** and the individual spectra of the species in the various protonation states were calculated by the computer program PSEQUAD.[67] Spectrophotometric titrations were performed on samples containing the ligands at 49 μM

Table 3 Crystal data and details of data collection for **1–6**

Compound	1	2	3	4	5	6
Empirical formula	$C_{10}H_{11}Cl_4CuN_5O_4S$	$C_{11}H_{17}Cl_4CuN_5O_6S$	$C_{18}H_{21}Cl_4CuN_5O_5S$	$C_{10}H_{11}Cl_4CuN_5O_4S$	$C_{13}H_{19}Cl_4CuN_5O_5S$	$C_{18}H_{23}Cl_4CuN_5O_6S$
Fw	502.64	552.70	624.81	502.64	562.73	642.83
T [K]	120	120	120	120	120	120
Space group	$P2_1/c$	$P2_1/c$	$P2_1/n$	$P2_1/c$	$P\bar{1}$	$P2_1/n$
a [Å]	13.8439(9)	7.5477(3)	9.5794(11)	10.0981(7)	8.9820(6)	9.4329(4)
b [Å]	11.9326(9)	17.3408(6)	17.6082(16)	21.8935(15)	9.8523(6)	20.2920(8)
c [Å]	11.6222(7)	15.7754(6)	15.4996(15)	17.1161(12)	13.4982(9)	14.1277(5)
α [°]	90.0	90.00	90.00	90.00	103.683(3)	90.00
β [°]	110.322(3)	95.6740(10)	105.502(4)	106.756(3)	94.647(3)	99.180(2)
γ [°]	90.0	90.00	90.00	90.00	110.613(3)	90.00
V [Å³]	1800.4(2)	2054.62(13)	2519.3(4)	3623.4(4)	1068.42(12)	2669.58(18)
Z	4	4	4	8	2	4
ρ_{calcd} [g cm^{-3}]	1.854	1.787	1.647	1.843	1.749	1.599
μ [mm^{-1}]	1.949	1.724	1.414	1.937	1.656	1.339
Crystal size [mm]	0.08 × 0.08 × 0.15	0.20 × 0.15 × 0.12	0.20 × 0.12 × 0.10	0.27 × 0.15 × 0.15	0.20 × 0.15 × 0.15	0.22 × 0.12 × 0.12
2Θ range	4.64 to 52.74	4.698 to 52.74	4.52 to 50.06	4.22 to 50.08	4.6 to 50.84	4.02 to 49.2
Reflections collected	35 405	30 340	29 389	82 072	67 667	61 193
Independent reflections	3672 [R_{int} = 0.0243]	4197 [R_{int} = 0.0421]	4441 [R_{int} = 0.0627]	6238 [R_{int} = 0.0332]	3924 [R_{int} = 0.0243]	4554 [R_{int} = 0.0431]
Data/restraints/parameters	3672/3/236	4197/0/255	4441/4/312	6328/0/453	3924/0/322	4454/3/318
$R_1{}^a$	0.0231	0.0270	0.0382	0.0223	0.0163	0.0240
$wR_2{}^b$	0.0561	0.0626	0.0888	0.0524	0.0427	0.0575
GOF^c	1.037	1.056	1.034	1.028	1.060	1.022
	0.37/−0.33	0.67/−0.46	1.03/−0.58	0.49/−0.50	0.35/−0.33	0.43/−0.32

^{a} $R_1 = \sum||F_o| - |F_c||/\sum|F_o|$. ^{b} $wR_2 = \{\sum[w(F_o{}^2 - F_c{}^2)^2]/\sum[w(F_o{}^2)^2]\}^{1/2}$. ^{c} $GOF = \{\sum[w(F_o{}^2 - F_c{}^2)^2]/(n-p)\}^{1/2}$, where n is the number of reflections and p is the total number of parameters refined.

concentration using a KOH solution in the presence of 0.1 M KCl at 25.0 ± 0.1 °C in the pH range from 2 to 12. An Orion 710A pH-meter equipped with a Metrohm combined electrode (type 6.0234.100) and a Metrohm 665 Dosimat burette were used for the pH-metric titrations. The electrode system was calibrated to the pH = −log[H⁺] scale by means of blank titrations (HCl vs. KOH) according to the suggested method.[68] The average water ionisation constant (pK_w) is 13.76 ± 0.05. Argon was also passed over the solutions during the titrations.

Complex formation of **HL¹** and **HL⁴** with copper(II) was studied by the methods of molar ratio and continuous variation at pH 4.07. Copper(II) stock solution was prepared by the dissolution of $CuCl_2$ in water and its concentration was determined by complexometry with EDTA. For the constant pH value of the samples an acetic acid/acetate buffer solution was used. The concentration of the ligand or the metal ion was constant (40 μM), while that of the other component was varied in the case of the molar ratio method. In addition, various metal-to-ligand ratios were also used, while the sum of the concentrations of the metal ion and the ligand was constant (100 μM). The conditional stability constants (β') of the investigated complexes were calculated at pH 4.07 based on the spectral changes via the displacement reaction with EDTA. In the competition experiments the samples contained 50 μM copper(II), and 50 μM ligand **HL¹** or **HL⁴**, and the concentration of EDTA was varied in the range from 0 to 72 μM. The conditional stability constants of the metal complexes (β' (CuL)) and the individual spectra of the species were calculated by the computer program PSEQUAD.[67] The overall stability constants (β) of the complexes [CuL]⁺ were calculated from the conditional stability constants: $\beta(CuL) = \beta'(CuL) \times \alpha_H$, where $\alpha_H = 1 + [H^+] \times \beta(HL) + [H^+]^2 \times \beta(H_2L)^+$ and $[H^+] = 10^{-4.07}$ M.

4.5 Electrochemistry measurements

Cyclic voltammetric experiments for **1–6** ($c_{1-6} = 10^{-3}$ M) in DMSO (SeccoSolv max. 0.025% H_2O, Merck) using nBu_4NPF_6 (puriss quality from Fluka; dried under reduced pressure at 70 °C for 24 h before use, $c = 0.1$ M) as a supporting electrolyte, were performed under an argon atmosphere in a one-compartment electrochemical cell with platinum wire as working and counter electrodes, and silver wire as a pseudo-reference electrode. Ferrocene purchased from Sigma Aldrich was used as the internal potential standard without further purification. All potentials in voltammetric studies were quoted vs. the ferricenium/ferrocene (Fc⁺/Fc) redox couple and controlled by using a Heka PG310USB potentiostat (Lambrecht, Germany, with the PotMaster 2.73 software package). Digital simulations of cyclic voltammograms were performed via DigiElch Professional software (version DigiElch8, Gamry Instruments, USA).

4.6 Antiproliferative activity (cell lines, culture conditions and MTT assay)

Cell lines and culture conditions. The human lung adenocarcinoma cells (A549), human breast cancer cells (MDA-MB-453), human colon cancer cells (LS174) and normal human bronchial

epithelial cells (BEAS-2B) were maintained as monolayer cultures in the Roswell Park Memorial Institute (RPMI) 1640 nutrient medium (Sigma Chemicals Co, USA). The RPMI 1640 nutrient medium was prepared in sterile ionised water, and supplemented with penicillin (192 IU mL⁻¹), streptomycin (200 mg mL⁻¹), HEPES (25 mM), L-glutamine (3 mM), and heat-inactivated fetal calf serum (FCS; 10%, pH 7.2). The cells were grown at 37 °C in CO_2 (5%) and humidified in air atmosphere, by twice weekly subculture.

MTT assay. The antiproliferative activity of the compounds was determined by using 3-(4,5-dimethylthiazol-yl)-2,5-diphenyltetrazolium bromide (MTT, Sigma Aldrich) assay.[69] Cells were seeded into 96-well cell culture plates (Thermo Scientific Nunc) in an appropriate density for each cell line. After 24 h of growth, cells were exposed to the serial dilutions of the tested compounds. The compounds were dissolved in dimethyl sulfoxide (DMSO) and afterwards diluted with the nutrient medium to the desired final concentrations. The amount of DMSO in the prepared solutions was ≤1%. Each concentration was tested in triplicate. After an incubation period of 48 h, MTT solutions (20 μL, 5 mg mL⁻¹ in phosphate buffer solution, pH 7.2) were added to each well. Samples were incubated at 37 °C with CO_2 (5%) in a humidified atmosphere for 4 h. Formazan crystals were dissolved in sodium dodecyl sulfate (SDS; 100 μM, 10%). Absorbance values were recorded after 24 h with an ELISA reader (ThermoLabsystem Multiskan EX 200–240 V) at the wavelength of 570 nm. The IC₅₀ values, defined as the concentrations of the compound causing 50% cell growth inhibition, were estimated from the dose–response curves.

Cell cycle analysis. The analysis of the cell cycle phase distribution was performed by flow cytometric analysis of the DNA content in fixed A549 cells, after staining with propidium iodide (PI).[70] Cells were seeded at a density of 2×10^5 cells per well, into 6-well plates (Thermo Scientific Nunc™), in 2 mL of the nutrition medium. Cells were continually exposed to the investigated complexes **3** and **6** or cisplatin at concentrations corresponding to IC₅₀, 1.5IC₅₀, and 2IC₅₀ for 24 h treatment and with IC₅₀ concentrations for 48 h treatment. Control cells were incubated only in a nutrient medium. After continuous treatment, all cells (detached and adherent) were collected, washed with phosphate-buffered saline (PBS), and fixed overnight in 70% ethanol. After fixation, cells were washed with PBS, and incubated with RNaseA (1 mg mL⁻¹) at 37 °C for 30 min. Just before flow cytometric analysis, cells were stained with PI, at a concentration of 400 μg mL⁻¹. The cell cycle phase distribution was investigated using a fluorescence activated cell sorter (FACS) Calibur Becton Dickinson flow cytometer and analysed by Cell Quest computer software.

Mechanism of cell death: analysis of apoptotic potential by annexin-V-FITC and PI staining. Flow cytometric analysis of the potential of **3**, **6** and cisplatin (reference compound) to induce apoptosis in A549 cells was performed using an annexin-V-FITC apoptosis detection kit, according to the manufacturer's instructions (BD Biosciences). The A549 cells (2×10^5) were seeded into 6-well plates (Thermo Scientific Nunc™), in 2 mL of RPMI medium. After 24 h of growth, cells were treated with

complexes or cisplatin for 24 or 48 h. After treatment, cells were washed with ice-cold PBS and then resuspended in 200 μL binding buffer (10 mM HEPES/NaOH pH 7.4, 140 mM NaCl, 2.5 mM $CaCl_2$). 100 μL of cell suspension (10^5 cells) was transferred to a 5 mL culture tube and mixed with 5 μL of annexin V-FITC and 5 μL of PI.[71] After incubation for 15 min, at 25 °C in the dark, 400 μL of binding buffer was added to each tube and analysed using a FACS Calibur Becton-Dickinson flow cytometer and Cell Quest computer software. A minimum of 10 000 cells were analysed per sample.

Morphological analysis of cell death by fluorescent microscopy: A549 cells (1×10^4) were seeded into 6-well plates (ThermoScientificNunc™) in 2 mL of nutrient medium. After 24 h of growth, cells were exposed to complexes 3 and 6, at $2IC_{50}$ concentrations. Following 24 h treatment, cells were stained with ethidium bromide (5 μg mL^{-1}) and acridine orange (1.5 μg mL^{-1}), according to the procedure reported elsewhere,[72] and immediately after, observed under the fluorescent microscope Axio Observer Z1, using AxioVision imaging software (Carl Zeiss MicroImaging GmbH).

Conflicts of interest

There are no conflicts to declare.

Acknowledgements

References

1 M.-C. Liu, T.-S. Lin and A. C. Sartorelli, *J. Med. Chem.*, 1992, **35**, 3672–3677.

2 A. M. Traynor, J. W. Lee, G. K. Bayer, J. M. Tate, S. P. Thomas, M. Mazurczak, D. L. Graham, J. M. Kolesar and J. H. A. Schiller, *Invest. New Drugs*, 2010, **28**, 91–97.

3 S. Wadler, D. Makower, C. Clairmont, K. Lambert, K. Fehn and M. Sznol, *J. Clin. Oncol.*, 2004, **22**, 1553–1563.

4 M. J. Mackenzie, D. Saltman, H. Hirte, J. Low, C. Johnson, G. Pond and M. J. Moore, *Invest. New Drugs*, 2007, **25**, 553–558.

5 J. F. Zeidner, J. E. Karp, A. L. Blackford, B. D. Smith, I. Gojo, S. D. Gore, M. J. Levis, H. E. Garraway, J. M. Greer, S. P. Ivy, K. W. Pratz and M. A. McDevitt, *Haematologica*, 2014, **99**, 672–678.

6 https://clinicaltrials.gov/ct2/show/NCT02433626, accessed on 24/06/2017.

7 K. Y. Salim, S. M. Vareki, W. R. Danter and J. Koropatnick, *Oncotarget*, 2016, **7**, 41363–41379.

8 (a) D. Rogolino, A. Cavazzoni, A. Gatti, M. Tegoni, G. Pelosi, V. Verdolino, C. Fumarola, D. Cretella, P. G. Petronini and M. Carcelli, *Eur. J. Med. Chem.*, 2017, **128**, 140–153; (b) Y. Gou, J. Wang, S. Chen, Z. Zhang, Y. Zhang, W. Zhang and F. Yang, *Eur. J. Med. Chem.*, 2016, **123**, 354–364.

9 D. Denoyer, S. Masaldan, S. La Fontaine and M. A. Cater, *Metallomics*, 2015, **7**, 1459–1476.

10 J. Easmon, G. Puerstinger, G. Heinisch, T. Roth, H. H. Fiebig, W. Holzer, W. Jaeger, M. Jenny and J. Hofmann, *J. Med. Chem.*, 2001, **44**, 2164–2171.

11 M. N. M. Milunovic, E. A. Enyedy, N. V. Nagy, T. Kiss, R. Trondl, M. A. Jakupec, B. K. Keppler, R. Krachler, G. Novitchi and V. B. Arion, *Inorg. Chem.*, 2012, **51**, 9309–9321.

12 M. B. Zeglis, V. Divilov and J. S. Lewis, *J. Med. Chem.*, 2011, **54**, 2391–2398.

13 S. Adsule, V. Barve, D. Chen, F. Ahmed, Q. P. Dou, S. Padhye and F. H. Sarkar, *J. Med. Chem.*, 2006, **49**, 7242–7246.

14 F. Bacher, É. A. Enyedy, N. V. Nagy, A. Rockenbauer, G. M. Bognár, R. Trondl, M. S. Novak, E. Klapproth, T. Kiss and V. B. Arion, *Inorg. Chem.*, 2013, **52**, 8895–8908.

15 J. T. Wilson, X. Jiang, B. C. McGill, E. C. Lisic and J. E. Deweese, *Chem. Res. Toxicol.*, 2016, **29**, 649–658.

16 A. Sîrbu, O. Palamarciuc, M. V. Babak, J. M. Lim, K. Ohui, E. A. Enyedy, S. Shova, D. Darvasiová, P. Rapta, W. H. Ang and V. B. Arion, *Dalton Trans.*, 2017, **46**, 3833–3847.

17 Saswati, A. Chakraborti, S. P. Dash, A. K. Panda, R. Acharyya, A. Biswas, S. Mukhopadhyay, S. K. Bhutia, A. Crochet, Y. P. Patil, M. Nethaji and R. Dinda, *Dalton Trans.*, 2015, **44**, 6140–6157.

18 C. Duncun and A. R. White, *Metallomics*, 2012, **4**, 127–138.

19 D. Palanimuthu, S. V. Shinde, K. Somasundaram and A. G. Samuelson, *J. Med. Chem.*, 2013, **56**, 722–734.

20 M. Gaba and C. Mochan, *Med. Chem. Res.*, 2016, **25**, 173–210.

21 E. Pahontu, F. Julea, T. Rosu, V. Purcarea, Y. Chumakov, P. Petrenco and A. Gulea, *J. Cell. Mol. Med.*, 2015, **19**, 865–878.

22 T. Riedel, O. Demaria, O. Zava, A. Joncic, M. Gilliet and P. J. Dyson, *Mol. Pharmaceutics*, 2018, **15**, 116–126.

23 S. Dhar and S. J. Lippard, *Proc. Natl. Acad. Sci. U. S. A.*, 2009, **106**, 22199–22204.

24 A. Kumar, S. Kant and S. M. Singh, *Chem.-Biol. Interact.*, 2012, **199**, 29–37.

25 S. Bonet, S. L. Archer, J. Allalunis-Turner, A. Haromy, C. Beaulieu, R. Thompson, C. T. Lee, G. D. Lopaschuk,

L. Puttagunta, G. Harry, K. Hashimoto, C. J. Porter, M. A. Andrade, B. Thebaud and E. D. Michelakis, *Cancer Cell*, 2007, **11**, 37–51.

26 W. Cao, S. Yacoub, K. T. Shiverick, K. Namiki, Y. Sakai, S. Porvasnik, C. Urbanek and C. J. Rosser, *Prostate*, 2008, **68**, 1223–1231.

27 B. M. Madhok, S. Yeluri, S. L. Perry, T. A. Hughes and D. G. Jayne, *Br. J. Cancer*, 2010, **102**, 1746–1752.

28 R. C. Sun, M. Fadia, J. E. Dahlstrom, C. R. Parish, P. G. Board and A. C. Blackburn, *Breast Cancer Res. Treat.*, 2010, **120**, 253–260.

29 W. Fiebiger, U. Olszewski, E. Ulsperger, K. Geissler and G. Hamilton, *Clin. Transl. Oncol.*, 2011, **13**, 43–49.

30 J. Tong, G. Xie, J. He, J. Li, F. Pan and H. Liang, *J. Biomed. Biotechnol.*, 2011, **2011**, 740564.

31 W. Y. Sanchez, S. L. McGee, T. Connor, B. Mottram, A. Wilkinson, J. P. Whitehead, S. Vuckovic and L. Catley, *Br. J. Cancer*, 2013, **108**, 1624–1633.

32 Y. C. Shen, D. L. Ou, C. Hsu, K. L. Lin, C. Y. Chang, C. Y. Lin, S. H. Liu and A. L. Cheng, *Br. J. Cancer*, 2013, **108**, 72–81.

33 K. Kumar, S. Wigfield, H. E. Gee, C. M. Devlin, D. Singleton, J. L. Li, F. Buffa, M. Huffman, A. L. Sin, J. Silver, H. Turley, R. Leek, A. L. Haris and M. Ivan, *J. Mol. Med.*, 2013, **91**, 749–758.

34 (*a*) http://clinicaltrials.gov/show/NCT01111097; (*b*) E. D. Michelakis, G. Sutendra, P. Dromparis, L. Webster, A. Haromy, E. Niven, C. Maguire, T. L. Gammer, J. R. Mackey, D. Fulton, B. Abdulkarim, M. S. McMurtry and K. C. Petruk, *Sci. Transl. Med.*, 2010, **2**, 31ra34.

35 M. Usman, F. Arjmand, R. A. Khan, A. Alsalme, M. Ahmad and S. Tabassum, *RSC Adv.*, 2017, **7**, 47920–47932.

36 D. C. Reis, A. A. R. Despaigne, J. G. da Silva, N. F. Silva, C. F. Vilela, I. C. Mendes, J. A. Takahashi and H. Beraldo, *Molecules*, 2013, **18**, 12645–12662.

37 I. Antonini, F. Claudi, P. Franchetti, M. Grifantini and S. Martelli, *J. Med. Chem.*, 1977, **20**, 447–449.

38 O. Dömötör, N. V. May, K. Pelivan, T. Kiss, B. K. Keppler, C. R. Kowol and E. A. Enyedy, *Inorg. Chim. Acta*, 2018, **472**, 264–275.

39 T. K. Venkatachalam, G. K. Pierens and D. C. Reutens, *Magn. Reson. Chem.*, 2014, **52**, 98–105.

40 V. I. Stenberg, P. A. Barks, D. Bays, D. Hammargren and D. V. Rao, *J. Org. Chem.*, 1968, **33**, 4402–4406.

41 M. Joseph, V. Suni, M. R. P. Kupur, M. Nethaji, A. Kishore and S. G. Bhat, *Polyhedron*, 2004, **23**, 3069–3080.

42 S. Indoria, T. S. Lobana, D. Singh, S. Kumari, P. Kumari, T. Bala, A. Kamal, A. K. Jassal, I. G. Santos, A. Castineiras and J. P. Jasinski, *Eur. J. Inorg. Chem.*, 2015, 5106–5117.

43 A. E. Stacy, D. Palanimuthu, P. V. Bernhardt, D. S. Kalinowski, P. J. Jansson and D. S. Richardson, *J. Med. Chem.*, 2016, **59**, 8601–8620.

44 E. A. Enyedy, N. V. Nagy, E. Zsigó, C. R. Kowol, V. B. Arion, B. K. Keppler and T. Kiss, *Eur. J. Inorg. Chem.*, 2010, 1717–1728.

45 J. Felcman and J. J. R. F. da Silva, *Talanta*, 1983, **30**, 565–570.

46 V. V. Pavlishchuk and A. W. Addison, *Inorg. Chim. Acta*, 2000, **298**, 97–102.

47 A. A. Shaikh, J. Firdaws, S. Serajee, M. S. Rahman and P. K. Bakshi, *Int. J. Electrochem. Sci.*, 2011, **6**, 2333–2343.

48 E. Ukpong and C. Obadimo, *Int. J. Electrochem. Sci.*, 2014, **9**, 4405–4412.

49 D. B. Rorabacher, *Chem. Rev.*, 2004, **104**, 651–697.

50 M. E. Manzanera-Estrada, M. Cruz-Ramírez, M. Flores-Alamo, J. M. Gracia y Jiménez, R. Galindo-Murillo, J. C. García-Ramos, L. Ruiz-Azuara and L. Ortiz-Frade, *J. Inorg. Biochem.*, 2017, **175**, 118–128.

51 R. Wopschall and I. Shain, *Anal. Chem.*, 1967, **39**, 1514–1527.

52 R. W. Byrnes, M. Mohan, W. E. Antholine, R. X. Xu and D. H. Petering, *Biochemistry*, 1990, **29**, 7046–7053.

53 M. A. Cater, H. B. Pearson, K. Wolyniec, P. Klaver, M. Bilandzic, B. M. Paterson, A. I. Bush, P. O. Humbert, S. la Fontaine, P. S. Donnelly and Y. Haupt, *ACS Chem. Biol.*, 2013, **8**, 1621–1631.

54 R. Ruiz, B. Garcia, J. Garcia-Tojal, N. Busto, S. Ibeas, J. M. Leal, C. Martins, J. Gaspar, J. Borras, R. Gil-Garcia and M. Gonzales-Alvarez, *J. Biol. Inorg. Chem.*, 2010, **15**, 515–532, DOI: 10.1007/s00775-009-0620-7.

55 M. del Carmen Aguirre, J. Borras, A. Castineiras, J. M. Garcia-Monteagudo, I. Garcia Santos, J. Niclos and D. X. West, *Eur. J. Inorg. Chem.*, 2006, 1231–1244.

56 P. J. Jansson, P. C. Sharpe, P. V. Bernhardt and D. R. Richardson, *J. Med. Chem.*, 2010, **53**, 5759–5769.

57 C. R. Kowol, P. Heffeter, W. Miklos, L. Gille, R. Trondl, L. Cappellacci, W. Berger and B. K. Keppler, *J. Biol. Inorg. Chem.*, 2012, **17**, 409–423.

58 B. Čobeljić, M. Milenković, A. Pevec, I. Turel, M. Vujčić, B. Janović, N. Gligorijević, D. Sladić, S. Radulović, K. Jovanović and K. Anđelković, *J. Biol. Inorg. Chem.*, 2016, **21**, 145–162.

59 G. Gasser, S. Grgurić-Šipka, M. Espina, M. Corte-Rodrıguez, L. Aguado, M. Montes-Bayon, M. I. Sierra, P. Martınez-Camblor, E. Blanco-Gonzalez and M. Sierra, *Metallomics*, 2017, **9**, 564–574.

60 M. M. Milutinović, A. Rilak, I. Bratsos, O. Klisurić, M. Vraneš, N. Gligorijević, S. Radulović and Ž. D. Bugarčić, *J. Inorg. Biochem.*, 2017, **169**, 1–12.

61 H. Zhang, R. Thomas, D. Oupicky and F. Peng, *J. Biol. Inorg. Chem.*, 2008, **13**, 47–55.

62 D. Wlodkowic, W. Telford, J. Skommer and Z. Darzynkiewicz, *Methods Cell Biol.*, 2011, **103**, 55–98.

63 C. Renvoize, A. Biola, M. Pallardy and J. Breard, *Cell Biol. Toxicol.*, 1998, **14**, 111–120.

64 *SAINT-Plus, version 7.06a, and APEX2*, Bruker-Nonius AXS Inc., Madison, WI, 2004.

65 O. V. Dolomanov, L. J. Bourhis, R. J. Gildea, J. A. K. Howard and H. Puschmann, *J. Appl. Crystallogr.*, 2009, **42**, 339–341.

66 G. M. Sheldrick, *Acta Crystallogr., Sect. C: Struct. Chem.*, 2015, **71**, 3–8.

67 L. Zékány and I. Nagypál, in *Computational Methods for the Determination of Stability Constants*, ed. D. L. Leggett, Plenum Press, New York, 1985, pp. 291–353.

68 H. M. Irving, M. G. Miles and L. D. Pettit, *Anal. Chim. Acta*, 1967, **38**, 475–488.

69 R. Supino, *In vitro Toxicity Testing Protocols*, Springer, New York, 1995, pp. 37–149.

70 M. G. Ormerod, *Analysis of DNA-General Methods. Flow Cytometry, a Practical Approach*, Oxford University Press, New York, 1994, p. 119.

71 M. van Engeland, L. J. W. Nieland, F. C. S. Ramaekers, B. Schutte and C. P. M. Reutelingsperger, *Cytometry*, 1998, **31**, 1–9.

72 S. Nikolić, L. Rangasamy, N. Gligorijević, S. Aranđelović and S. Radulović, *J. Inorg. Biochem.*, 2016, **160**, 156–165.